CHALMERS

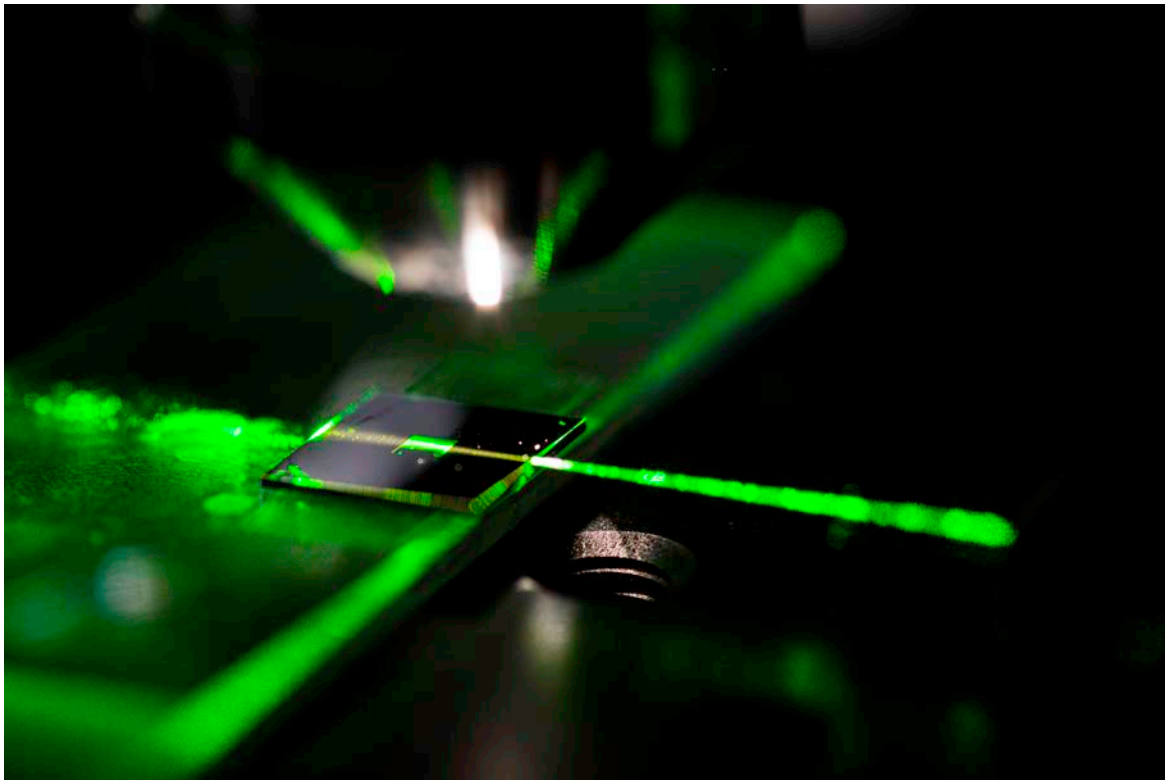

Single Molecule Detection using Optical Waveguide

Master's Thesis in Applied Physics

MATHIAS ELMESKOG

Department of Applied Physics
Division of Biological Physics
Chalmers University of Technology
Gothenburg, Sweden 2013

THESIS FOR THE DEGREE OF MASTER OF SCIENCE

Single Molecule Detection using Optical Waveguide

MATHIAS ELMESKOG

Department of Applied Physics
Division of Biological Physics
Chalmers University of Technology
Gothenburg, Sweden 2013

Single Molecule Detection using Optical Waveguide

MATHIAS ELMESKOG

©MATHIAS ELMESKOG, 2013

Department of Applied Physics
Division of Biological Physics
SE-412 96 Gothenburg
Sweden
Telephone +46(0)31-772 10 00

Printed at Chalmers Reproservice Gothenburg, 2013

Cover illustration: *In the image on the front page the optical waveguide platform is illuminated by a 532 nm laser from the side. Here the waveguide is placed on the stage of a upright microscope and a 20x objective used for alignment purposes. The platform is a three layer symmetric optical waveguide with a etched well at the center. This well is 2 by 2 mm and* $\approx 3\,\mu\text{m}$ *deep.* ©*Mathias Elmeskog*

Single Molecule Detection using Optical Waveguide

MATHIAS ELMESKOG
Department of Applied Physics
Division of Biological Physics
Chalmers University of Technology
Gothenburg, Sweden 2013

Abstract

Molecular interactions with single molecule sensitivity is a growing field with application in pharmaceutical development and diagnostics. Existing techniques that can be used for single molecule interaction studies, such as total internal reflection fluorescence (TIRF) microscopy are often expensive and complicated to use. They also have critical limitations, for example the need of labeling with fluorophores.

In this thesis a novel method based on a single mode optical waveguide is investigated for surface binding with single molecule sensitivity. A three layer planar waveguide is used where the core layer is a light carrier. The refractive index of the cladding layers are matched to that of water in order to make it compatible with measurements in a liquid environment. Mounted under a regular upright microscope, the evanescent field in the waveguide can be used for excitation of fluorophores or for monitoring the scattering intensity. In this project the latter method was used exclusively. It was shown 20 nm gold nano particles bound to, or very close to, the core layer surface of the optical waveguide could be visualized. The ability to perform real time measurements makes it possible to determine if a gold nano particle binds reversibly or irreversibly to the surface. The possibility to functionalize the core layer surface in different ways has also been studied.

The concept was further developed into a biosensing technique using an antibody sandwich assay to detect amyloid-β peptides at very low concentrations. This is of interest due to amyloid-β peptides suspected role in developing plaque in brain tissue which lead to Alzheimer's disease. To be able to detect traces of this peptide in blood plasma at an early stage could help develop techniques to inhibit or stop the development process of the disease. It was found to be possible to detect amyloid-β 1-37, 1-37 indicates the number of amino acids in the peptide, down to at least a concentration of 100 fM in the bulk solution added to the waveguide chip using the waveguide technique.

Keywords: Optical waveguide, evanescent field, single molecule sensitivity, surface sensitive measurement, biosensing, Alzheimer's disease, amyloid-β peptide.

Acknowledgements

I would like to take the opportunity to thank all the people who have not only made this project possible but also fun and personal rewarding.

Fredrik Höök my main supervisor and examiner. For giving me the opportunity to do this project and be a part of this scientific adventure. All the insights and discussions not only about the project but also intriguing and sometimes quite strange topics.

Björn Agnarsson for all the support and help with everything! Thank you. And the pizza at Foxes.

Anders Lundgren for immense patience of a physicists ignorance towards chemistry and biology. All the guidance and hands on training in the lab, insights and knowledge.

Biological Physics Group for the openness and warmth making it easy to go to work. For making me not once hesitate to ask a question to anybody in the group and always getting an enthusiastic answer back. For the "fika" breaks with all the good discussions and laughs.

Friends It is quite convenient to have most of your closest friends grouped up and in the same boat. Long studying days that sometimes gets longer due to completely unrelated discussions sometimes they get shorter due to great teamwork and sharing of knowledge. Looking back later in my life I will most certainly remember these years as laughs and fun times. This is because of you.

Family The road to get to this point have been all but straight. For the love over the years the support in tough times and pushing me to continue.

Ewa for the understanding, love and support late evenings and early sundays when work have been necessary. And kissing in the staircase.

Mathias Elmeskog, Gothenburg, 22 September 2013

Contents

1

Introduction

Biological physics is a fast growing field of study with enormous potential. It spans from studying single molecule interactions to construction of mind controlled mechanical hand prosthesis [1]. In the quest for knowledge, human kind strives to study the extremes of any unit scale irrespective if it is length, time, speed or concentration. To achieve this, scientist develop tools in cunning ways to measure and observe passages of events which their own senses lack the ability to comprehend.

1.1 Background and Motivation

"Why do we do this?" is a question my supervisor Björn Agnarsson often remind me to have in back of my mind. This will not only keep the work on the right track it will also make sure that the work we do have some kind of meaning. In this small section the work done is motivated from both the point why this is important in a lager picture and the advantages it has compared to other available techniques.

1.1.1 Alzheimer's Disease

Alzheimer's disease is the most common form of dementia in the world today with approximately 20-30 million cases [2, 3]. The clinical signs are behavioral changes, progressive cognitive deterioration and memory loss. It is believed that peptide amyloid-β accumulates in brain tissue in the earliest stages of the disease [3]. This makes it much desired to measure this accumulation of amyloid-β. Unfortunately it is quite late in the dementia process that these plaques become visible in scans with the techniques available today. It is suggested that high levels of amyloid-β42 or the ratio amyloid-β42/amyloid-β40 in plasma is a strong indicator for future risk to develop Alzheimer's disease [4]. However there are reports that conclude the opposite and this could be according to H. Zetterberg, professor of neurochemistry at Gothenburg University, *"...due to the fact that Aβ42 is notoriously difficult to measure in plasma."* [2].

The diagnosis of Alzheimer's disease is a difficult process even with technology available today and it includes many different aspects, including brain scans, blood tests, analyzing patient

medical history, studies of behavioral changes and medical revisits. To make any of these steps easier, or to be able to find a method that can replace two or more of this components would simplify this process a lot. There are today no available treatments for Alzheimer's disease but there have been progress and there is hope for using low-density lipoprotein receptor–related protein-1 (LRP) to clear amyloid-β from the brain [5].

In this work an attempt to develop a surface based technique to detect amyloid-β peptides at very low concentration is presented using an optical waveguide platform.

1.1.2 Techniques for Measurement of Molecular Interactions used Today

There are several established techniques for measurement of molecules binding to a surface, two of these are quartz crystal microbalance with dissipation (QCM-D) and surface plasmon resonance (SPR). These two techniques were used in this work as reference techniques and it will be shown that they have some crucial limitations compared to the optical waveguide technique. The most important one is the sensitivity region, which will be described later in this report.

In the optical waveguide system an evanescent field is used to make measurements surface sensitive. Why and how this evanescent field is created is presented in chapter 2. Total internal reflection fluorescence (TIRF) is another technique that uses evanescent fields in measurements. The technique used in this work relates very much to TIRF but has some advantages over TIRF, as it is cheaper and simpler, it has a larger area of illumination, and the penetration depth can be tuned. The most important difference is that in the waveguide system the molecules do not have to be stained with fluorophore. For an in depth text on TIRF the reader is referred to a text by Daniel Axelrod [6].

There are other techniques to observe gold nano particles on a surface, one example is dark field microscopy but they have some crucial limitations. With TIRF and the waveguide system there is the possibility to measure during the binding process. This is not possible with dark field microscopy because the solution on top of the sample must be rinsed before the surface becomes visible. Also the gold nano particles must be much larger compared to the gold nano particles that can be used in the waveguide system in order to be observed, the limit size for observation in dark field microscopy is about 60 nm. This is quite large relative to the particles that can be seen in the waveguide system making the particles less affected by gravity and have faster diffusion rate.

1.2 Thesis Outline

The author has a background in physics making it natural if this reflects in the thesis. Some parts about chemistry and biology is quite basic while some areas of physics and mathematics is not explained in depth.

Chapter 2 - Evanescent-Waveguide In this chapter the optical waveguide platform is explained. The physics behind the exponential decaying evanescent wave is also discussed. The experimental setup used in this work is explained.

Chapter 3 - Biological Foundation In order to understand and be able to analyze the results, some basic knowledge about biological systems is useful. This chapter is an introduction to molecular dynamics and theoretical models for molecular binding to surfaces.

Chapter 4 - Reference Techniques The techniques used for characterization and reference are explained from a theoretical standpoint and their relevance for this thesis.

Chapter 5 - Materials and Methods This section explains the experiments, material used and preparations of the measurements.

Chapter 6 - Results In this chapter the results are briefly presented and explained.

Chapter 7 - Discussion Here the results are discussed in more depth. Also reflections and thoughts of the preparation steps are discussed and how they could effect the results.

Chapter 8 - Conclusions The conclusions drawn from the work is presented.

Chapter 9 - Future Perspective During the time working with this project a lot of thoughts on how to further develop the method. In this chapter some of the ideas are presented. Also suggestions of further measurements validating the presented work are discussed.

2

Evanescent-Waveguide

The main method during this thesis is an evanescent waveguide technique for measurements on biological systems in liquid environments. In this chapter the three layer waveguides structure and functionality will be discussed more in depth. Since the core layer, the layer where the measurements are done, is a spin on glass material that is in surface properties very similar to silicon dioxide glass on the surface after plasma treatment the possibilities for surface modification and functionalization of various kinds are many.

2.1 Optical Theory for Waveguides

An optical waveguide is a structure of materials with different refractive indices that confines light within its core. The most common and used waveguide is an optical fiber that has a large area of use, from signal transfers to house decorations. A propagating wave in the core creates an exponentially decaying evanescent field at the edge of the core layer and into the surrounding material as shown in figure 2.1. This evanescent tail can be used to visualize nano particles close to the surface.

Figure 2.1: *Structure of a layer slab planar waveguide. n1, n2 and n3 are the refractive indices of the different materials. The thickness of the core layer is* $2a$ *with x-coordinate zero at the center of the core layer (the green layer).*

2.1.1 Maxwell's Equations

When for example a gold nano particle is very close to the core layer surface the particle will scatter light. This scattered light comes from the evanescent field from the wave guide. To understand where the evanescent field comes from and how light behave in a waveguide structure there is natural to look at Maxwell's equations.

Since the layers are non-magnetic and non-conductive material the reduced Maxwell's equations can be used,

$$\nabla \cdot \mathbf{E} = 0 \tag{2.1}$$

$$\nabla \cdot \mathbf{H} = 0 \tag{2.2}$$

$$\nabla \times \mathbf{E} = -\mu_0 \frac{\partial \mathbf{H}}{\partial t} \tag{2.3}$$

$$\nabla \times \mathbf{H} = \epsilon \frac{\partial \mathbf{E}}{\partial t} \tag{2.4}$$

where $\mathbf{E}$ is the electrical field, $\mathbf{H}$ the magnetic field, ϵ the media permittivity and μ_0 permeability. Using the vectorial formula $\nabla\times(\nabla\times\mathbf{E}) = \nabla(\nabla\cdot\mathbf{E})-\nabla^2\mathbf{E}$ with the simplified Maxwell's equations a two vectorial wave equations called the *homogeneous wave equations* can be derived

$$\nabla^2 \mathbf{E} = \mu_0 \epsilon \frac{\partial^2 \mathbf{E}}{\partial t^2} \tag{2.5}$$

$$\nabla^2 \mathbf{H} = \mu_0 \epsilon \frac{\partial^2 \mathbf{H}}{\partial t^2}. \tag{2.6}$$

There are a infinite number of possible solutions for these equations. Using the *harmonic wave solution*, $\mathbf{E}(\mathbf{r},t) = \mathbf{E}(\mathbf{r})e^{i\omega t}$, on the homogeneous wave equations the Helmholtz equation is obtained that describes the electric and magnetic field distribution in the structure. Since the interesting field is the electric field the rest of this derivation will concentrate on that. Helmholtz electric field distribution equation then can be written as

$$\nabla^2 \mathbf{E}(\mathbf{r}) + k^2 n^2(\mathbf{r}) \mathbf{E}(\mathbf{r}) = 0 \tag{2.7}$$

where $k = \frac{\omega}{c}$, ω is the angular frequency, c is the speed of light in vacuum and $n(\mathbf{r})$ the refractive index distribution. The wave propagation in z-direction is approximated as a plane wave propagation the expression can be rewritten as

$$\mathbf{E}(\mathbf{r}) = \mathbf{E}(x,y)e^{-i\beta z} \tag{2.8}$$

where β is a propagation constant for the wave along the propagating axis z. Combining this with the Helmholtz equation for the electric field the following expression can be derived

$$\frac{\partial^2 \mathbf{E}(x,y)}{\partial x^2} + \frac{\partial^2 \mathbf{E}(x,y)}{\partial y^2} + \frac{\partial^2 \mathbf{E}(x,y)}{\partial z^2} + (k^2 n^2(\mathbf{r}) - \beta^2)\mathbf{E}(x,y) = 0 \tag{2.9}$$

In this thesis a flat three layer waveguide is constructed confining the light only in the x-direction. Using equation (2.9) the electric field distribution can be derived for the separate

layers. Assuming that the thickness of the core layer is $2a$ with $x = 0$ at the center of the core layer.

$$\frac{\partial^2 \mathbf{E}(x,y)}{\partial x^2} + (k^2 n_1^2 - \beta^2)\mathbf{E}(x,y) = 0 \quad x > a \tag{2.10a}$$

$$\frac{\partial^2 \mathbf{E}(x,y)}{\partial x^2} + (k^2 n_2^2 - \beta^2)\mathbf{E}(x,y) = 0 \quad -a < x < a \tag{2.10b}$$

$$\frac{\partial^2 \mathbf{E}(x,y)}{\partial x^2} + (k^2 n_3^2 - \beta^2)\mathbf{E}(x,y) = 0 \quad x < -a \tag{2.10c}$$

The top layer and the bottom layers are called cladding layers. In the cladding layers there is an expected exponential decay which is the evanescent field. Choosing appropriate boundary conditions equation 2.10 can be solved.

$$E_y = \begin{cases} A\cos(\delta a - \phi)e^{-\sigma(x-a)} & x > a \\ A\cos(\delta x - \phi) & -a \leq x \leq a \\ A\cos(\delta a + \phi)e^{\xi(x+a)} & x < -a \end{cases} \tag{2.11}$$

where A is a non determined constant, ϕ a phase constant and δ, σ, ξ are constants that are related to the refractive indices of the layers and given by the expressions below.

$$\delta = \sqrt{k_0^2 n_2^2 - \beta^2} \tag{2.12a}$$

$$\sigma = \sqrt{\beta^2 - k_0^2 n_1^2} \tag{2.12b}$$

$$\xi = \sqrt{\beta^2 - k_0^2 n_3^2} \tag{2.12c}$$

As can be seen from equation 2.11 the electric field decays exponentially into the cladding layers with a decay length given by the equations 2.12. The exponential decay makes this a very surface sensitive technique.

2.1.2 Characteristics of Symmetric Waveguides

In equation 2.11 it can be noticed that the evanescent field does not have to be symmetric around the center of the core layer. This depends on the refractive indices of the cladding layers. A symmetric waveguide has the same refractive index in both cladding layers [7]. The theory behind this can of course be looked at in more depth but here the very basics are explained.
The penetration depth is defined as where the electric field amplitude has dropped to $1/e$ of it's value on the surface. Using this the penetration depth can be written as[7]

$$d = \frac{\lambda}{2\pi} \frac{1}{\sqrt{n_{eff}^2 - n_{cladding}^2}} \tag{2.13}$$

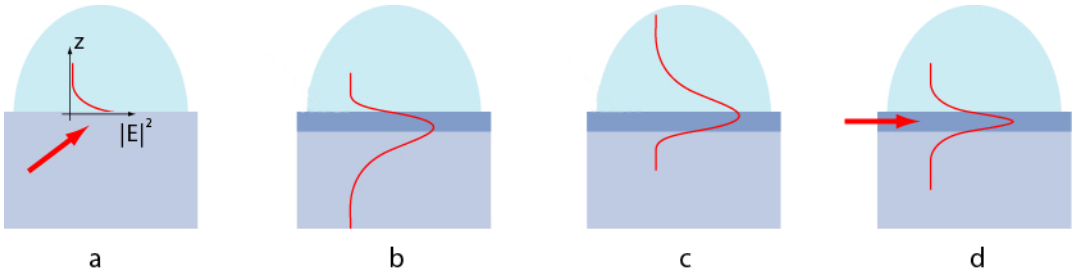

Figure 2.2: *The different characteristics of the evanescent field depending on the refractive indices of the different layers.* ***(a)*** *Total internal reflection in the substrate.* ***(b-d)*** *Characteristics of the excitation field depending on the refractive index with* ***(b)*** *higher,* ***(c)*** *lower and* ***(d)*** *approx. the same as the refractive index of the sample solution. Image used with permission from Björn Agnarsson [7].*

where λ is the wavelength of the connected laser and n_{eff} is the effective refractive index of the waveguide mode. The effective refractive index can be calculated numerically from the Maxwell's equations 2.10

$$n_{eff} = \frac{c\beta}{\omega} \tag{2.14}$$

For a single mode waveguide and typical wavelength and effective refractive index the penetration depth will be in order of 100-200 nm.

A symmetric waveguide structure has some crucial advantages compared to an asymmetric structure. A large variety of polymers can be used as cladding layers and thereby it is possible to tune the penetration depth. This can also be accomplished be varying the geometric structure of the waveguide, for example core thickness. The illumination area is quite big making it possible to do measurements on a larger area. But probably the main advantage with this end-fire evanescent waveguide platform is that measurements on a single molecule attached on for example a gold nano particle can be done, this means that measurements can be made label free. To be able to do measurements label free have a number of advantages, for example that labels bleach during measurements and may alter the functionality of the measured molecule.

2.2 Experimental Setup

The basic setup for the experiments is very easy including a regular microscope, 532 nm laser and computer which are all commercially available, the tricky part is the custom made waveguide. Even though the setup is easy, it is to this day quite hard to use for an unexperienced user. In this section the main components will be discussed and their importance for the setup.

The microscope that was used was an upright Olympus BX61 microscope that has a high accuracy z-axis stage for optimal focus abilities. The lenses used were a 2x and 20x for alignment of laser fiber and waveguide, a 100x wet objective with the numerical aperture of 1.0 was used for measurements.
ImageJ, a free software, was used to control the microscope, stage and camera. A setup of micro screws was setup to be able to very precise align the optical laser fiber. This is critical for the experiment and good measurements. This alignment had to be adjusted continuously not to lose signal.

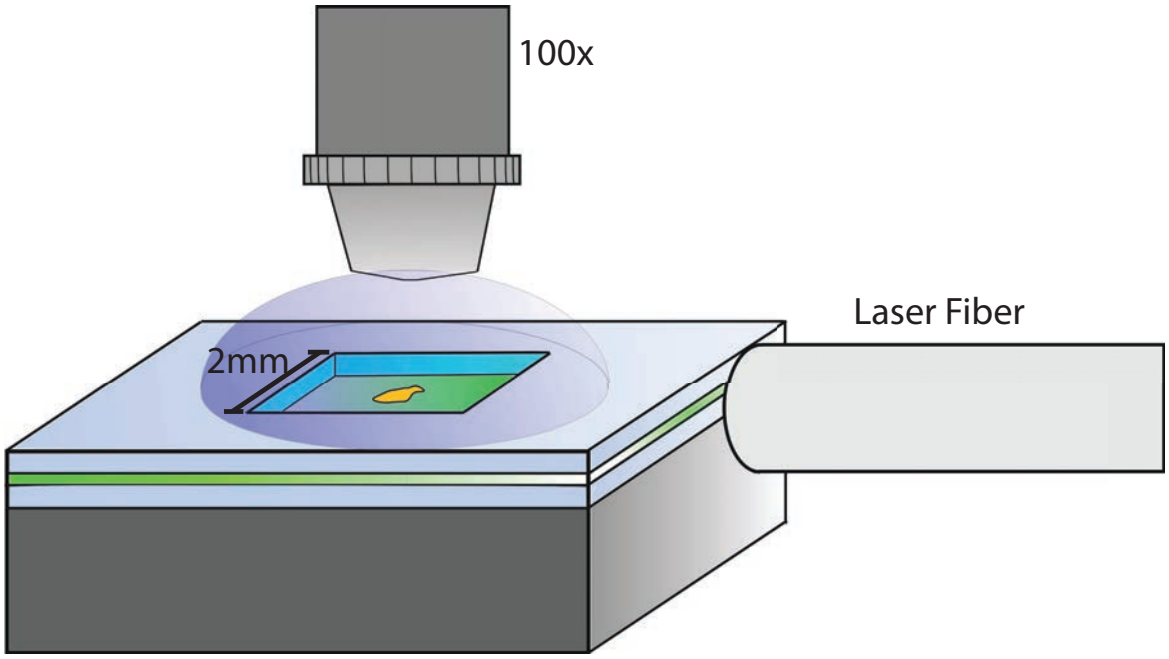

Figure 2.3: *Schematic view of the waveguide system used. The laser comes in from the right and the fiber is aligned for the best possible connection to create a good evanescent field. There are three layers on the silicon wafer, the bottom layer is a CYTOP which is a polymer, the middle layer is the core layer which is spin on glass, the top layer is a CYTOP layer equal to the bottom layer. In the middle of the chip a well is etched through the CYTOP down to the core layer. The well is* 2 mm *by* 2 mm *and approximative* 3 µm *deep which also is the thickness of both CYTOP layers. All measurements was done with liquid on the well and a 100x liquid immersed objective with a numerical aperture of 1.0.*

3

Biological Foundation

BIOLOGICAL PHYSICS spans a large range of topics but in general methods from physics is just used to understand and answer biological questions. In this chapter a short overview of the biological foundations for this thesis is presented. Simple structures of biological membranes, surface functionalization and molecule binding dynamics is discussed. In this thesis a measuring technique of peptides is investigated with the goal of ultra high sensitivity technique for measuring amyloid β peptides for Alzheimer's disease diagnostics. Therefore an introduction to Alzheimer's disease is presented.

3.1 Vesicles and Lipid Bilayers

All living organisms are built by biological cells which is a structure with different function groups, contained by a protecting membrane. The size of a cell vary in the region of 1 - 100 µm[8]. This membrane, and what it contains, have a huge impact on the functionality of the cell and thereby life itself. The membrane makes a barrier to the outside world protecting the cell but it must also enable the passage of vital nutrients in to the cell and allow waste materials to get out se figure 3.1. At the same time it must be flexible and durable to allow cell movement, division and growth. For this reason there is of great importance to understand the structure of the membrane and how it works.

The biological cell membrane is a structure of self assembled lipid molecules that have hydrophobic tails and a hydrophilic head, see figure 3.2a. To minimize the free energy of the aqueous lipid solution the hydrophilic head will screen the hydrophobic tails from the water molecules and spontaneous aggregates are formed [8]. These aggregates can make different shapes for example spheres, vesicles (spherical shells) and supported layers depending on parameters like critical chain length, optimum head group area and lipid concentration [9]. It is now easy to assume that the lipids are fixed which is not the case, they are constantly moving around in the membrane like a two dimensional liquid. Applying force to this kind of structure will reshape it and rip it apart if the force is too big. Calculations on membrane deformation is a very interesting topic but will not be further discussed in this thesis, for a deeper insight in the subject see the book "Physical Biology of the Cell" [8].

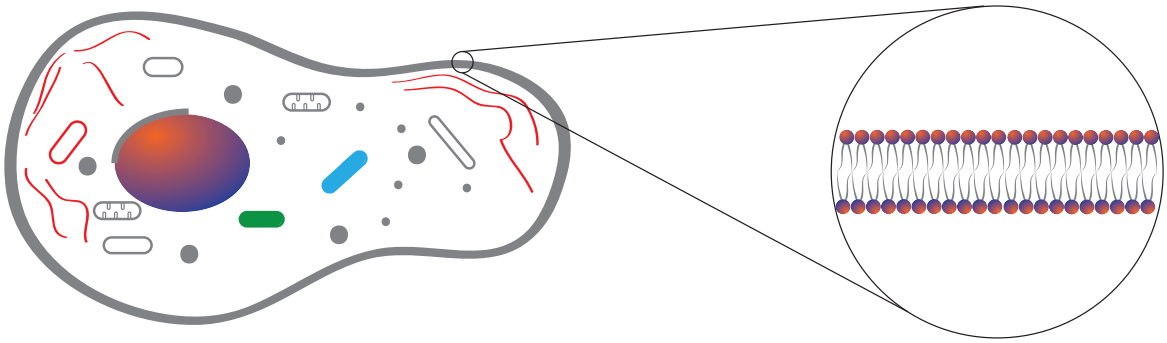

Figure 3.1: *Simple sketch of a Eukaryotic cell with the cell nucleus and different function groups. There are many types of membrane structures with embedded proteins but the one here magnified is a lipid bilayer called plasma membrane.*

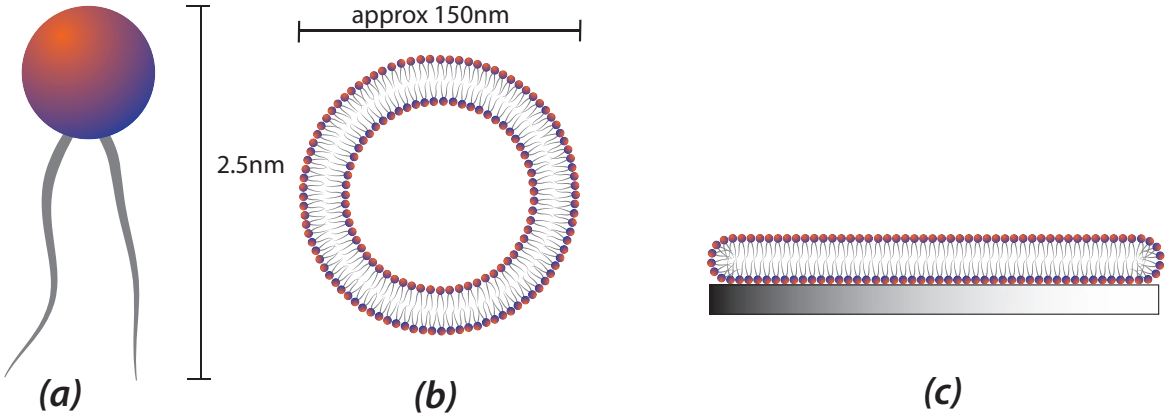

Figure 3.2: (a) *Lipid molecule with hydrophobic tails and hydrophilic head that creates a structure about* 2.5*nm long. There are many different type of lipids but since the most important for this thesis is the phospholipid which have two tails to one head group this will be for the illustration.*(b) *Self assembled lipid vesicle, which is a spherical shell. The size of a vesicle can very different and they can be made in many different sizes. In the work represented here they are approx.* $100 - 150\,\mathrm{nm}$. (c) *A supported lipid bilayer on for example* SiO_2. *Both the lipid bilayer and the vesicle are about* 5*nm thick.*

Functional proteins are embedded in the membrane giving the membrane some of its functionality enabling interactions between the surroundings and inner structure of the cell. Some of these proteins are just embedded on the top layer of the membrane and some go right through it. The interactions and dynamics of interactions are discussed further in the next section.

3.2 Ligand-Receptor Kinetics

In this section the goal is to understand and build a statistical model system of two different molecules binding to each other. This model will help interpreting results and data, and is especially important for single molecule binding experiments. To create a model system it is often a good idea to start with the easiest scenario. In this case that means that no account will be taken to what molecules are interacting. See figure 3.3 for a graphical representations

that will be used in this section. This fairly basic model is a great tool in biology and binding dynamics and as will be shown later on show the competition between translational entropy and binding energy for biology relevant solution systems.

3.2.1 Ligand-Receptor Interaction

In this thesis single molecule interactions are monitored and therefore knowledge about the nature of biological interactions are relevant. In the most fundamental case of molecular binding between a ligand (L) and a receptor (R) a new complex is formed (LR). With a large affinity between the ligand and receptor the complex will stay this way and not separating. However if the affinity is low they will separate again to form a free ligand and receptor and be open for new interactions. When time goes towards infinity this will create a equilibrium between free ligands and receptors and the complex LR, this is represented by the equation:

$$L + R \underset{k_{off}}{\overset{k_{on}}{\rightleftharpoons}} LR \tag{3.1}$$

where k_{off} and k_{on} are kinetic rate constants for the forward and reverse reactions and are described by the equation [10]

$$\frac{dLR}{dt} = k_{on}[L][R] - k_{off}[LR] \tag{3.2}$$

where the square brackets indicate concentrations. These equations can be investigated further for relevant relations but they are not relevant for this thesis and left for the reader to read if interested [8].

Figure 3.3: *Representations of two different molecules that are able to react with each other with the receptor to the left and the ligand to the right.*

3.2.2 Ligand-Receptor Dynamics

One case scenario is when there is only one receptor but many ligands in the system. Using this and a mathematical grid representing the possible locations for the ligands in the solution, different microstates is created with different configurations enabling the possibility for statistical calculations, see figure 3.4. The number of microstates can be expressed as

$$N_{microstates} = \frac{\Omega!}{L!(\Omega - L)!} \tag{3.3}$$

where Ω is the number of lattice sites and L the number of ligands. The main goal here is to derive a mathematical model to calculate the probability for a ligand to be bound to the

receptor as a function of the ligand concentration. Here it comes natural to construct a ratio between the number of microstates where one ligand has bound to the receptor divided with the total number of microstates. There are a few different ways this can be achieved and here the Botzmann distribution and partition function are chosen.

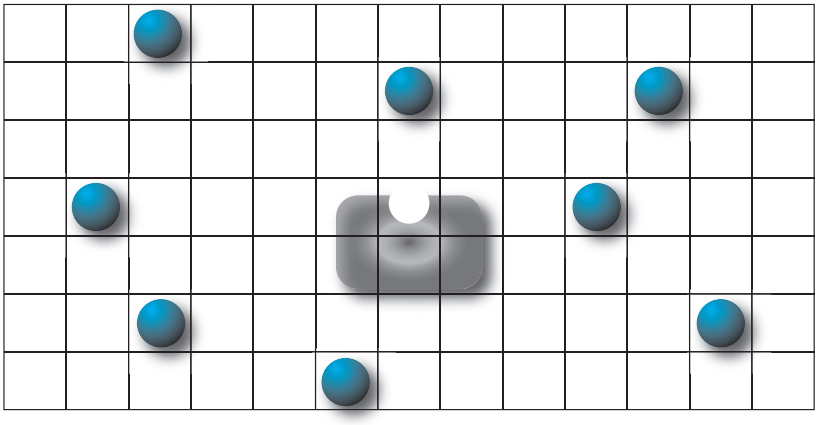

Figure 3.4: *Grid representation of ligand receptor solution. The number of ligands are L the number of lattice sites are Ω and one receptor.*

The probability for a ligand to be bound to a receptor is p_{bound} and here it is very important to understand and a key for this derivation that there are only two classes of states. The first one contains all microstates where the receptor is not occupied and the second one is all the microstates where the receptor is occupied. Using this the weight of the states can be calculated as

$$W_{receptoroccupied} = e^{-\beta\epsilon_b} \sum_{solution} e^{-\beta(L-1)\epsilon_{sol}} \tag{3.4}$$

where the first exponential term is the bound ligand and the sum is the free ligands in the solution, ϵ_b is the binding energy for the bounden ligand and ϵ_{sol} is the energy of the free ligands in the solution. Since the Boltzmann factor is the same for all ligands in the solution arranging $(L-1)$ ligands on Ω lattice sites the sum can be written as

$$\sum_{solution} e^{-\beta(L-1)\epsilon_{sol}} = \frac{\Omega!}{(L-1)!(\Omega-(L-1))!} e^{-\beta(L-1)\epsilon_{sol}} \tag{3.5}$$

The sum of *all* possible microstates is the partition function and is given by

$$Z(L,\Omega) = \sum_{solution} e^{-\beta L\epsilon_b} + e^{-\beta\epsilon_b} \sum_{solution} e^{-\beta(L-1)\epsilon_{sol}} \tag{3.6}$$

where the first sum is for the non-bound ligands and the second sum is for the bound ligands in the different microstates. The second sum is already evaluated in equation 3.5. With the same approach for the first sum the sum can be written as:

$$\sum_{solution} e^{-\beta L\epsilon_{sol}} = e^{-\beta L\epsilon_{sol}} \frac{\Omega!}{L!(\Omega-L)!} \tag{3.7}$$

Using the two equations 3.5 and 3.7 and putting them in the partition function yields

$$Z(L,\Omega) = \frac{\Omega!}{L!(\Omega-L)!}e^{-\beta L\epsilon_{sol}} + \frac{\Omega!}{(L-1)!(\Omega-(L-1))!}e^{-\beta(L-1)\epsilon_{sol}}e^{-\beta L\epsilon_b} \tag{3.8}$$

if $L \ll \Omega$ the simplification $\frac{\Omega!}{(\Omega-L)} \approx \Omega^L$ can be used. And now all components to write down p_{bound} are found

$$p_{bound} = \frac{\frac{\Omega^{L-1}}{(L-1)!}e^{-\beta L\epsilon_b}e^{-\beta(L-1)\epsilon_{sol}}}{\frac{\Omega^L}{L!}e^{-\beta L\epsilon_{sol}} + \frac{\Omega^{L-1}}{(L-1)!}e^{-\beta L\epsilon_b}e^{-\beta(L-1)\epsilon_{sol}}}. \tag{3.9}$$

By defining $\Delta\epsilon = \epsilon_b - \epsilon_{sol}$ and multiplying both the numerator and denominator with $(L!/\Omega^L)e^{\beta L\epsilon_{sol}}$ this equation can be further reduced to

$$p_{bound} = \frac{\frac{L}{\Omega}e^{-\beta\Delta\epsilon}}{1+\frac{L}{\Omega}e^{-\beta\Delta\epsilon}}. \tag{3.10}$$

The last step now is to convert this to an equation depending on concentrations. The volume of the solution is $V_{solution}$ which leads to the ligand concentration as $c = L/V_{solution}$ and a reference concentration as $c_0 = \Omega/V_{solution}$

$$p_{bound} = \frac{(c/c_0)e^{-\beta\Delta\epsilon}}{1+(c/c_0)e^{-\beta\Delta\epsilon}}. \tag{3.11}$$

This equation goes under many different names such as Langmuir adsorption isotherm and Hill function [8]. The characteristics of the curve created by this equation is very similar to figure 3.7 which is derived from the special case of this type of dynamics and is called The Langmuir Model and will be discussed in depth in the following section.

3.2.3 The Langmuir Model

In the optical waveguide system, and reference methods, used in this thesis the receptors will be immobilized on a surface. This will allow the usage of the Langmuir model, which is a special case of ligand-receptor dynamics theory, that describes how surface adsorptions of molecules relates to molecular concentrations. By creating a relation between the amount of receptors on the surface (Θ_{max}) and a time dependent amount of bound ligands to a receptor ($\Theta(t)$) the relative surface coverage can be calculated as $\Theta(t)/\Theta_{max}$.

When adding a solution of ligands to the surface with the immobilized receptors ligands will start to bind to the receptors, see figure 3.5a. The relative surface coverage will get higher until the system has reached an equilibrium, see figure 3.5b. Equation 3.2 can be used to describe the kinetics of this system, a graphical representation of surface coverage is seen in figure 3.6. The kinetic parameters k_{on} and k_{off} together with the law of mass action can be described as the differential equation

$$\frac{d\Theta(t)}{dt} = k_{on}C(\Theta_{max}-\Theta(t)) - k_{off}\Theta(t) \tag{3.12}$$

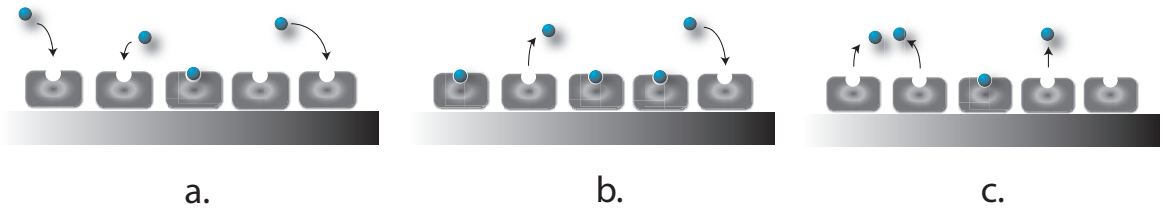

Figure 3.5: *Illustration of the surface coverage over time. In (a) the ligands are injected in the solution starting to bind to the receptors. (b) an equilibrium is reached between ligands binding in to the receptor and ligands releasing creating the maximum coverage of the system. (c) ligands are removed from the bulk solution by for example rinsing lowering the relative surface coverage.*

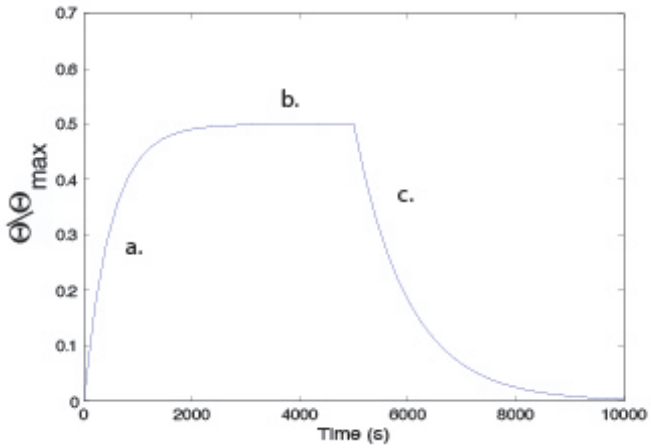

Figure 3.6: *A graphical representation of the relative surface coverage based on the Langmuir theory. (a), (b) and (c) represent the same stages as in figure 3.5. Figure used with permission from Olov Wahlsten, Biological Physics, Chalmers University of Technology.*

where C is the ligand concentration in the solution. Rearranging 3.12 with the time dependent components to one side and non time dependent components to the other yields

$$\frac{d\Theta(t)}{dt} + \Theta(t)(k_{on}C + k_{off}) = k_{on}C\Theta_{max} \tag{3.13}$$

which is a quite straight forward equation to solve using a integrating factor $\sigma(t)$ and applying the chain rule for derivation. By using a exponential integrating factor $\sigma(t) = e^{(k_{on}C+k_{off})t}$ this equation can be solved

$$\frac{d}{dt}(e^{(k_{on}C+k_{off})t}\Theta(t)) = k_{on}C\Theta_{max}e^{(k_{on}C+k_{off})t} \tag{3.14}$$

By integrating both sides of this equation and setting the initial condition $\Theta(0) = 0$ (since the surface coverage is zero before any ligands have been injected in the solution) the solution for the equation can be expressed as

$$\Theta(t) = \frac{k_{on}C\Theta_{max}}{k_{on}C + k_{off}}(1 - e^{-(k_{on}C+k_{off})t}) \tag{3.15}$$

Figure 3.7 show how the surface coverage is related to change in ligand concentration.

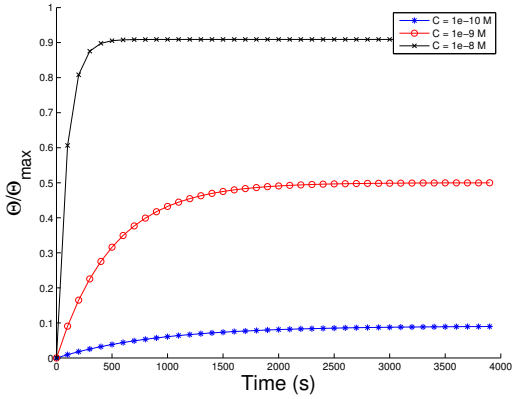

Figure 3.7: *The calculated curves for equation 3.15 representing the relative surface coverage at three ligand concentrations. The kinetic constants k_{on} and k_{off} is set to $10^6\,(\mathrm{sM})^{-1}$ and $10^{-3}\,\mathrm{s}^{-1}$ respectively.*

When $t \to \infty$ the ratio $\Theta(t)/\Theta_{max}$ is at equilibrium and the equilibrium coverage can be written as

$$\frac{\Theta(t)}{\Theta_{max}} = \frac{k_{on}C}{k_{on}C + k_{off}} = \frac{C}{C + K_d} \tag{3.16}$$

where K_d is k_{off}/k_{on}. This result is known as the Hall-Langmuir equation and K_d is interpreted as the concentration where the coverage is at 50% of the coverage maximum at equilibrium, see figure 3.8.

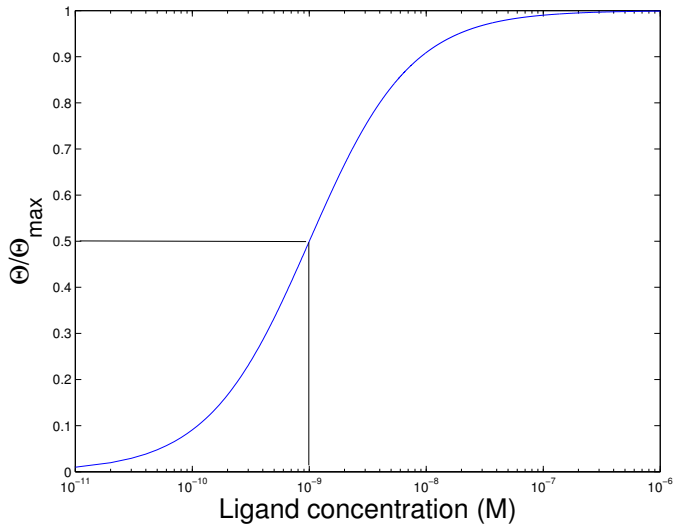

Figure 3.8: *The relative surface coverage as a function of ligand concentration in the solution which is a result of the Hall-Langmuir equation 3.2.3. By reading this graph at $\Theta/\Theta_{max} = 0.5$ the result for K_d is obtained and in this case it is $10^{-9}\,\mathrm{M}$.*

3.3 Biological Functionalization of Surfaces

Receptors are immobilized on surfaces by functionalization of the surface. Methods depending on what type of native surface is used and what kind of reactions are expected when a solution is added to the surface. There are numerous of methods to achieve this, and here two main methods are used. One is to form a lipid bilayer containing the receptors on the surface and no reactions with the surface will happen and the second one is silanization of a glass surface that will react with the silicon in the glass making the surface extremely reactive. This gives the ability to immobilize receptors on the surface.

3.3.1 Creating a Functionalized Supported Lipid Bilayer

To understand this type of surface functionalization one must know a little more about self assembly. In this section some equations will just be stated without any derivation, so the reader must either trust the author or read a book or course in condensed soft matter physics.

As mentioned in previous sections the main component of a biological membrane are lipids with a hydrophobic tail and a hydrophilic head group. How these lipids aggregate and self assemble is mainly dependent on the concentration of lipids and they will assemble in a way that will minimize the free energy in the solution. Since the main objective here is to understand bilayer formation, the focus will be on self assembly of vesicles and bilayers even though they may take may other shapes like spheres or rods. It is always good to have a mathematical theory to fall back on and that explains when and why physical phenomena occurs when different parameters are changed. A good starting point is to see whether it is energetically favorable for the lipids to self assemble or not. The following equation turns out to be a powerful tool.

$$X_N = N\left[X_1 e^{\frac{(\epsilon_1-\epsilon_N)}{k_B T}}\right]^N. \tag{3.17}$$

This equation can be used to calculate the volume fraction X_N of solute molecules in an aggregate with N molecules. ϵ_N is the energy change when a single lipid molecule is taken from the bulk solution and put in this aggregate. The free solute molecule fraction is X_1 and ϵ_1 is the free energy of a single molecule. T is the temperature in Kelvin and k_B the Boltzmann constant.

Now the interpretation of this equation is straight forward. If $\epsilon_N \geq \epsilon_1$ then the most molecules in the solution will be isolated molecules, on the other hand if $\epsilon_N < \epsilon_1$ the molecules will aggregate and the system will have a lower free energy. Depending on what kind of lipid composition there is in the solution the molecules will aggregate more or less easily. Phospholipids form aggregates easily into vesicles structures due to the fact that they have two tails creating small values of critical chain length but keeping large hydrocarbon volume together with a optimum head group area. ϵ_N is very dependent on the shape of the aggregate formed, the different shapes will have different surface energy for example which is one factor in the free energy model.

For a sheet like structure as in figure 3.2 *(c)* equation 3.17 can be written as

$$X_N = N\left[X_1 e^{\alpha}\right] e^{-\alpha N^{1/2}} \tag{3.18}$$

$$\alpha = \frac{\sqrt{N}(\epsilon_N - \epsilon_\infty)}{k_B T}. \tag{3.19}$$

ϵ_∞ comes from the fact that the sheet is handled as if it is infinite. This is of course not the case since there must be a higher free energy at the edges of the sheet. For vesicles on a surface to form a supported lipid bilayer instead of staying as vesicles on the surface it most be energetically favorable for the system. Since the edges of a supported lipid bilayer have a relative high free energy the bilayer will only form if the sheet is big enough to be energetically favorable see figure 3.2 *b*.
By doing this reversed a supported lipid bilayer can be created on a surface by applying a solution with a high concentration of vesicles.

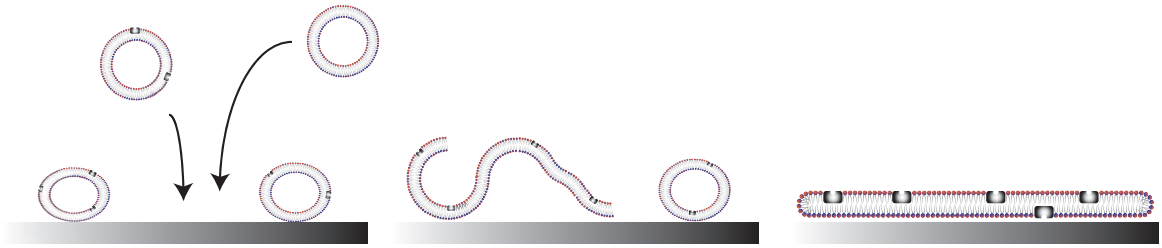

Figure 3.9: *When adding a solution containing vesicles, that have receptors in the membrane, they will land on the surface as shown in the first stage. As it gets crowded on the surface the vesicle will start to fuse and opens up. If there is enough vesicles landing on the surface a bilayer will be created with the embedded receptors. The receptors have now been immobilized for experiments with added ligands.*

To be able to create lipid bilayers on the wave guide surface does not only indicate that the surface has many desired properties it also works as a functionalization of the surface. The lipid bilayer can be used as a platform for many different platforms for example membrane protein behavior. In figure 3.10 there is a comparison between lipid bilayer formation in QCM-D and the waveguide system. The different steps that can be seen in figure 3.9 is observed as changes in the measurement in figure 3.10.

3.3.2 Silanization of Glass Surfaces

Silanization is a functionalization to make the surface very reactive. This is done by creating a self assembled monolayer on a mineral surface containing hydroxyl groups like glass. In figure 3.11 the chemical structure of (3-aminopropyl)-diethoxy-methylsilane (APDMES) silane bound to a SiO_2 surface that was used in this work. Glutaraldehyde bind to the NH_3 groups and on top of that the antibody is immobilized.

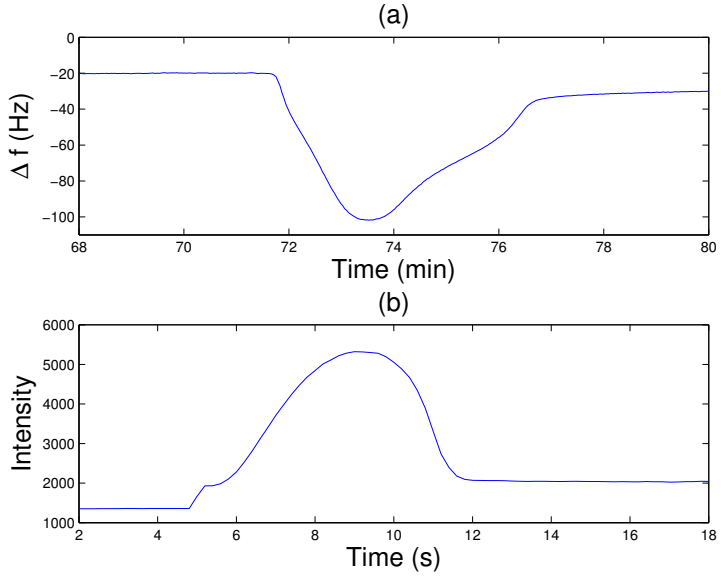

Figure 3.10: *Results for bilayer formation in waveguide and QCM-D experiments. (a) is the result from QCM-D measurement. When the vesicles land on the crystal surface the frequency goes down until a critical point of surface coverage is reached and the vesicles collapse to a lipid bilayer and the frequency goes back up. (b) is the intensity measurement for the waveguide experiment and here it is the same principle but instead of frequency the intensity is measured and where the frequency goes down the scattering intensity goes up.*

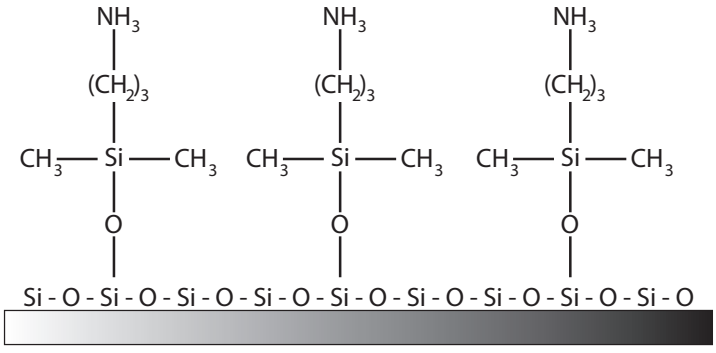

Figure 3.11: *Chemical structure of bound (3-aminopropyl)-diethoxy-methylsilane (APDMES) to a SiO_2 surface.*

3.4 Introduction to Alzheimer's Disease

Alzheimer's disease is a neurologic disorder in the brain and the first documented case with the specific name was presented by Alois Alzheimer in 1906. He discovered plaques in the brain and he called them "military bodies" and dense bundles of fibrils. It was not until 1985 than researchers succeeded to purify plaques in the brain, and investigated the main components of this plaques. It was a 4 kD amyloid-β peptide [11]. This peptide has been proposed to be the

driving force in the disease process [4]. Alzheimer's disease is a huge research area so this section will just be a short introduction of the disease and its mechanisms.

3.4.1 Structures and Properties of Amyloid-β Peptides

Amyloid-β is a peptide with a defined length of 36-43 amino acids. The different lengths of the peptide gives it different properties and are therefore grouped in smaller categories. The amyloid-β is formed by sequential cleavage of amyloid precursor protein that is present in many different tissues but can mainly be found in synapses of neurons. The peptide have no defined structure or folding and therefore it will not crystallize.

3.4.2 Development and Effects on the Brain with Alzheimer's Disease

As mentioned the most common theory for what is behind the progress of Alzeimer's disease is accumulation of amyloid-β plaques in the brain effecting the functionality of the brain. This causes dementia and since there is no cure the patient effected will get worse and eventually die.

3.4.3 Available Treatments and Diagnostics

Diagnosing potential patients with Alzheimer's disease is today not a straight forward medical test. There is a long process with many different aspects to it, with blood tests, brain scans, analyze of medical history and repeated examination of behavioral changes. Since it is thought that the main reason for this declining function of the brain is due to accumulation of peptide in the brain forming plaques it is much desired to solve this problem. This can be done by preventing plaques to form and degrade plaques that already have been formed.

Today there are no cure for Alzheimer's disease, there are just medication and other treatments helping some of the symptoms like sleep deprivation, dementia and behavioral changes. They do not treat the cause of Alzheimer's disease just damp the symptoms. There are treatments that are under development that could treat what is believed to be the cause, and that is the plaques in the brain. This could be done by using low-density lipoprotein receptor–related protein-1 (LRP) to clear amyloid-β from the brain [5].

4

Reference Techniques

To verify results obtained with a new method and characterize result data a complementary technique, preferable a well established one, can be used as a reference. In this project where a new technique for measurement of molecular binding to a surface is developed there have been two main complementary techniques, Quartz Crystal Microbalance with Dissipation monitoring (QCM-D) and Surface Plasmon Resonance (SPR). Nano-particle Tracking Analysis (NTA) have been used to characterize the gold nano particles used in the experiments. In this chapter these three methods are briefly explained.

(a) QCM-D (b) BIAcore 2000 SPR

Figure 4.1: *The two main complementary devises to characterize and for referent measurements.* ***(a)*** *A Q-Sense E4 QCM-D device. (Image with permission from q-sense.com)* ***(b)*** *The BIAcore 2000 SPR that was used in this work.*

4.1 QCM-D - Quartz Crystal Microbalance with Dissipation monitoring

QCM-D is an acoustic wave based measurement technique for quantifying adsorption on a surface which allows measurements of small mass changes and viscoelastic properties in real time. This

is achieved by measuring the frequency shift, caused by mass adsorption of molecules, on an oscillating quartz crystal. Quartz is a piezoelectric material that will deform with an external electrical field and will generate an electric field if deformed. When an alternating current, with an appropriate frequency, is applied to an AT[1] cut quartz crystal it will start to oscillate at its resonance frequency in a shear fashion as demonstrated in Figure 4.2. The resonance frequency is dependent on the thickness of the quartz crystal since the crystal is in resonance when the top and the bottom are in anti-phase[12]. This gives the condition that an odd multiple of $\lambda/2$ should match the thickness of the crystal to obtain resonance.

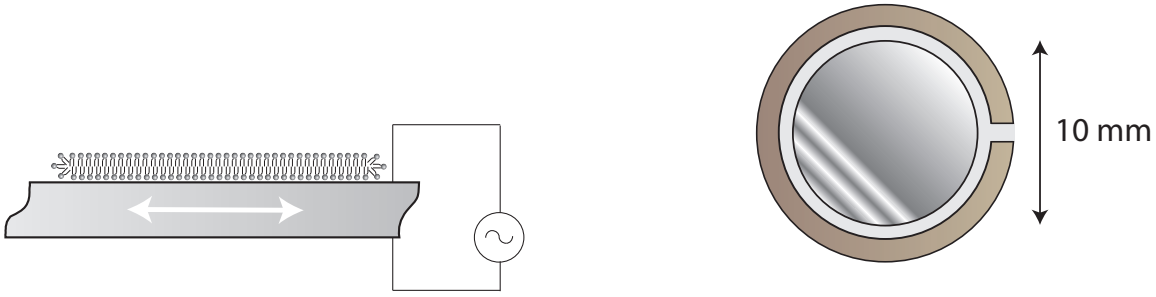

Figure 4.2: ***(a)*** *Shows a schematic overview of the QCM-D quartz crystal cross section. By applying an alternating voltage over the crystal it starts to oscillate as the arrows indicate. When the acoustic wave created is an odd multiple of $\lambda/2$ that matches the thickness of the crystal it fulfills the requirements for resonance.* ***(b)*** *Illustration of a QCM-D quartz crystal.*

The frequency shift of the resonance have a linear relation towards the adsorbed mass on the surface described by the Sauerbrey relation [13],

$$\Delta m = -\frac{C\Delta f}{n} \tag{4.1}$$

where Δf is the the frequency resonance shift, Δm is the change in mass due to adsorption to the surface, C is a crystal specific constant and for the regular 5 MHz crystal $C = 17.7\,\mathrm{ng/(Hzcm^2)}$ and n is the number of the harmonic used. Assuming that it is possible to make readout from acquired data as low as $\Delta f \approx 0.1\,\mathrm{Hz}$ the sensitivity of the system is around $1\,\mathrm{ng/cm^2}$. In spite of the high sensitivity for this technique it has a wide range for detectible molecular weights, from just a few hundred Da up to GDa [14].

The dissipation gives information about the viscoelastic properties of the adsorbed layer. If a complete rigid layer is applied there will be no shift in the dissipation for example a layer of gold, a soft layer will show a larger shift in the dissipation. This dissipation is monitored by turning the applied alternating voltage rapidly on and off continuously, while the potential is off the decrease of the oscillation amplitude is measured. This decrease in amplitude is a result of energy dissipating to surrounding media. Using this the dissipation D can be calculated[15],

$$D = \frac{1}{2\pi}\frac{E_{dissipated}}{E_{stored}} \tag{4.2}$$

[1] An AT cut crystal is a crystal that is cut at 35,25°with the optical axis.

where $E_{dissipated}$ is the energy loss for each oscillation while the potential is off and E_{stored} is the energy stored in the system.

4.2 SPR - Surface Plasmon Resonance

Surface Plasmon Resonance (SPR) is a highly sensitive measuring technique for surface adsorption and binding. Since SPR is a highly surface sensitive technique it makes a very good reference to the waveguide scattering system and are able to measure the same biological systems with a high sensitivity.

SPR measures the changes in surface plasmon resonance angle that occurs due to excitations of laterally propagating surface plasmons on planar metal surfaces, for example gold. The condition for plasmon resonance on the surface is extremely sensitive to changes of the interfacial refractive index, $\Delta n_{interface}$ [16]. $\Delta n_{interface}$ changes with adsorption of biomaterial on the surface and will give a change in surface plasmon resonance angle.

4.3 NTA - Nano-particle Tracking Analysis

In the waveguide scattering system, gold nano-particles are used for their ability to scatter light very efficiently. The NTA is used to characterize the nano-particles before and after modification to determine their size distribution. This gives not only information about the size and distribution of the size but also if the modification was successful and if the nano-particles have aggregated. Since the scattering is strongly dependent on the radius of a solid sphere nano-particle this is crucial.

Nano-particle Tracking Analysis (NTA) is based on measuring Brownian motion of nano-particles in a solution [17]. This is accomplished by shooting a laser beam through a prism with the solution on top, the the scattering signal of individual particles are recorded in a movie file using a regular microscope with a camera. The data is processed with a software that uses the two-dimensional Stokes-Einstein equation [18]

$$< x,y >^2 = \frac{K_B T_{t_s}}{3\pi\eta d_h}, \tag{4.3}$$

where $< x,y >^2$ is the mean square displacement, K_B the Boltzmann constant, T temperature of the system, η the viscosity of the solution, t_s the sampling time and d_h the hydrodynamic diameter of the nano particle.

5

Materials and Methods

During this thesis many different methods were used due to that the main method for this thesis is a newly developed method that have not yet been fully characterized. For this reason the reference methods will be extra important for interpretation of the data obtained. In this chapter the materials and methods used are explained. All chemicals are purchased from Sigma-Aldrich (USA) if not otherwise is stated. All water used was deionized and filtered using a MilliQ unit (Millipore, France). The buffer in all experiments was a phosphate buffered silane (PBS) that was prepared with 200 ml of milliQ water and a dissolved PBS tablet, the PBS was the degased.

5.1 Gold Nano Particles Fabrication and Coating

For all waveguide based measurements gold nano particles were used due to their ability to scatter 532 nm light very efficiently. For this gold nano particles coated with polyethylene glycol (PEG) containing biotin were fabricated. The size distribution for the gold nano particles before and after coating can be seen under results figure 6.1.

5.1.1 Fabrication of Gold Nano Particles

Fabrication of gold nano particles is quite straight forward. 1 µl tannic acid 1% was added to 32 ml of milliQ in a beaker, 8 ml sodium citrate 1% was mixed with 160 ml milliQ water. The two solutions were heated to 65 °C and then mixed in a larger beaker and kept at 65 °C with constant stirring. After 2.5 hour the temperature was raised to 95 °C for a 1.5 hour. By then the solution had reached a nice deep crimson red. The gold nano particle solution was then divided in four 50 ml falcon tubes and placed in the fridge.

5.1.2 Coating with Polyethylene Glycol

To make the gold nano particles stable and to prevent aggregation in a salt solution like PBS the gold nano particles were coated with polyethylene glycol (PEG). This also gives the opportunity to biotinylate the particles. Using a micro balance 0.006 g of PEG-COOH and 0.0015 g of PEG-Biotin were mixed with 1.5 ml milliQ water and distributed equal between three of the falcon tubes containing 50 ml gold nano particle each and left over night. Then the solution was

distributed in 30 1.5 ml vials and centrifuged 60 minutes at 5000 g. The pellet that was formed in the bottom of the vial was pipetted up and diluted to 1.5 ml again and centrifuged again the same way, this was repeated 5 times. After the last centrifugation the pellets were not diluted to create a stock solution.

5.2 Bilayer Formation

In order to test the waveguide surface it is good to compare bilayer formation in the different systems. The shape of measurement curves in the QCM-D forming bilayer is well documented and are therefor suitable for this kind of comparison see figure 3.10.

5.2.1 Bilayer Formation with QCM-D

A *Q-Sense E4* instrument was used and a commercially available SiO_2 (Q-Sense AB, Sweden) crystal was cleaned in UV-ozon oven for two times ten minutes with rinsing in milliQ water between. The crystal was then dried in a stream of nitrogen and mounted in the QCM-D chamber. PBS was used as a running buffer and the flow rate was 100 µl/min. Then 1 mg/ml POPC-PE:PEG-Biotin was injected and a bilayer was formed during flow.

5.2.2 Bilayer Formation with the Evanescent Waveguide Technique

The evanescent waveguide chip was plasma cleaned for ten minutes, then rinsed with milliQ and dried with a stream of nitrogen. After this cleaning procedure the chip was mounted under the microscope with a regular glass coverslip and double-sided tape. The laser was roughly aligned at the edge of the chip using naked eye. 20 µl of PBS was put on the well and a 100X wet objective was used to locate a suitable area for measurements. Laser alignment and power, exposure time, gain and focus was then optimized for measurement. Then 10 µl of 1 mg/ml POPC-PE:PEG-Biotin was added to the drop on the well and the bilayer formation was recorded.

5.3 NTA Concentration Characterization

The NTA is mainly made for size measurements for nano particles but here a small investigation was made to see if it is possible to use the NTA technique for concentration measurements. The NTA used was a Nanosight LM10 (Nanosight, England) and Nanosight 2.0 software. A stock solution with calculated concentration of 0.2 nM gold nano particles was diluted in a series 4/1000, 2/1000, 1/1000 and 1/2000. To see if there was any difference in the result measurements on both regular gold nano particles with a size of 30 nm and polyethylene glycol (PEG) chains on them and the size then goes up to 59 nm. Each sample was measured three times for 60 seconds for each measurement, the gain was set to 619, shutter 1495, blurr $5x5$ and the threshold was adjusted to only count particles that were in focus.

5.4 Immuno Assay for Amyloid β Detection

A immuno assay was developed for measurement of amyloid-β peptides and investigated with three different measurement techniques. Two that are commercial available and established and the new evanescent waveguide technique. The biological system is basically the same for all different measuring techniques and in figure 6.10 there is a sketch of the biological system.

5.4.1 QCM-D Preparation and Measurement

As mentioned in chapter 4 the QCM-D method is well established for surface measurements of biological structures. This makes it very good as a reference method. In all QCM-D measurements a *Q-Sense E4* instrument was used, purchased from Q-Sense AB, Sweden.

Commercial QCM-D Crystal

As a starting point, a commercially available QCM-D quartz crystal was used, coated with SiO_2 (Q-Sense AB, Sweden). Three crystals of the same kind was used and treated exactly the same except for the step when the peptide of interest was added so there was one positive control and two negative. The crystal was cleaned in a UV-ozon oven for $2 * 10$ minutes with rinsing with milliQ water between the cleaning and after. The crystal was thoroughly dried with a stream of N_2 and then put in a solution with 10% 3-Aminopropyldimethylethoxsilane (APDMES, abcr GMbH & Co. Germany) and 90% methanol that completely covered the the crystal, it was left for incubation for one hour. After one hour the crystal was first rinsed with methanol and then milliQ water. After the silanization the crystal incubated in a petri dish with PBS and 2% glutaraldehyde for 15 minutes.

After these functionalization steps of the surface the crystal was dried and quickly mounted in the QCM-D and the chamber was filled with PBS, which also was the running buffer at 100 µl/min. The antibody 6E10 (Covance, USA), with the concentration 50 µg/ml, was injected in the chamber and incubated for 20 minutes without flow. A short pulse of ,less then one minute at regular injection speed, ethanolamine was injected through the chamber at a high concentration (1M). Human serum albumin (HSA) was then injected with a concentration of 10 mg/ml and incubated without flow until no more adsorption could be measured. Then the peptide of interest was added, here channel three was used as a positive control and a solution with amyloid-β at 250 nM for 20 minutes no flow. After injection of the peptide in channel three the antibody 4G8 (Covance, USA) with the a concentration of 10 µg/ml was added until saturation. Streptavidin was injected at a concentration of 10 µg/ml for 15 minutes. The last step was to inject the biotinylated gold nano particles and measuring until saturation.

Spin on Glass Coated QCM-D Crystal

In the waveguide experiments the contact surface will be a spin on glass (SOG) material so to get a more accurate interpretation of the QCM-D results three crystals were coated with a 400 nm thick SOG film.

The crystals was then plasma cleaned for 10 minutes and rinsed in milliQ water. After this cleaning procedure the same steps as with the non coated crystal were taken. Crystals were functionalized with 10% APDMES and 90% methanol for 2 hours, rinsed with methanol and milliQ, put in a solution with PBS and 2% glutaraldehyde for 15 minutes, dried with a stream of nitrogen, mounted in QCM-D chambers, 6E10 at a concentration of 25 µg/ml for 50 minutes with no flow, ethanolamine 1M less then one minute, human serum albumin with the concentration 10 mg/ml 10 minutes incubation with no flow, amyloid-β 1-37 250 nM with channel three as a negative control, 4G8 with the concentration 10 µg/ml, streptavidin with the concentration 10 µg/ml and the last step was to inject the biotinylated gold nano particles and measure until saturation.

5.4.2 Evanescent Waveguide Preparation and Measurements

The really strong side of the QCM-D and the SPR is the flow systems were micro pumps will create flow over the surface, this will make the adsorption less sensitive for diffusion limitations of the binding. This is also a weakness because it requires quite a lot of material. Even though the steps of the antibody sandwich seen in figure 6.10 are quite the same small alterations between measurements will occur, they will be discussed in the discussion chapter. For a more in depth description of the experimental setup see chapter 2.2.

The waveguide chips were rinsed in milliQ water and dried in a stream of nitrogen before being plasma cleaned for 10 minutes and rinsed in milliQ again and dried thoroughly. 20 µl of 10% APDMES and 90% methanol were pipetted on the waveguide well after they had been placed in petri dishes. About 40 µl of pure methanol was placed at the edges of the petri dish and the lid was put on. The APDMES was incubated for one hour without any mixing. The chip was then rinsed with first methanol and then milliQ water and placed in a petri dish with 3 ml of 2% glutaraldehyde for 15 minutes. After the incubation the chip was rinsed in first PBS and milliQ and dried with nitrogen.

A 20 µl drop of PBS was placed on the well of the chip and 20 µl of 50 µg/ml 6E10 was pipetted in the PBS drop and incubated for one hour with hand mixing each five minutes with a pipet. The chip was then rinsed using 20 µl of PBS and mix and waste 16 times. 20 µl of HSA at a concentration of 10 mg/ml was injected in the drop on top of the well this was incubated for one hour without any mixing then rinsed 16 times with PBS. Ethanolamine was then injected and rinsed within one minute with 16 times of PBS. Then the amyloid-β was added at desired concentration and incubated for note nor with mixing each five minutes and rinsed 16 times with PBS. The second antibody biotynilated 4G8 was then added at a concentration of 50 µg/ml and a volume of 20 µl for one hour with mixing each five minutes and the same rinsing procedure as the other steps. The last step done on the lab bench is to add 20 µl streptavidin with the concentration 50 µg/ml for 30 minutes then rinsed 16 times with PBS.

After the preparations with building the biological system on the lab bench the chip was ready for measurements. The chip was placed under the microscope and laser roughly aligned with a high laser power (around 30 mW), then the well and a suitable area was located to be able to do this a 2X and 20X objective was used. To get good measurements it was important to put some time to optimize the parameters as focus, laser alignment and power, camera gain and exposure time. During all measurements a 100X wet objective was used.

A time laps was then started with one image per second to one image each ten seconds depending on the condition and suspected binding rate. The length of the measurement was depending on the binding rate but often around 1000 seconds. All measurements was saved as a stack of tiff-files and processed with MatLab (Mathworks, USA) and the free software *ImageJ*.

5.4.3 SPR Preparation and Measurements

The SPR used in my studies was a Biacore2000 (Biacore, Sweden) with standard gold surfaces. The machine run with PBS until stable baseline then the measurements was restarted for better readout. For surface functionalization a 1-Ethyl-3-(3-dimethylaminopropyl) carbodiimide (EDC) and N-Hydroxysuccinimide (NHS) coupling agents were used. 37.5 µl of 2 mg/ml EDC was

diluted to 150 µl and 5.72 µl of 2 mg/ml NHS was also diluted to 150 µl both using PBS. The two solutions were then mixed and 150 µl was injected over a period of 15 minutes. The antibody 6E10 was injected for 10 minutes with 10 µl/min at a concentration of 10 µg/ml. Ethanolamine was injected for one minute 10 µl/min at $1M$ then amyloid-β 1-37 at 250 nM 10 µl/min for ten minutes. The last step was to add the second antibody 4G8 for ten minutes with a flow of 10 µl/min at the concentration 10 µg/ml.

6

Results

In this chapter the main results obtained during this project are presented. Many different methods have been used to acquire and process the data. The two main softwares that were used for the processing of data are commercially available numeric mathematics software MATLAB and the free image processing software *ImageJ*. The results can be divided into two main parts. The first one is characterization of the waveguide and the second is an immune assay method for detection of peptide proteins in solution with the optical waveguide.

6.1 Gold Nano Particle Size and Visibility in Waveguide System

It is important to characterize the gold nano particles used in the experiments in order to be able to interpret the results correctly. The particle scatter intensity is strongly dependent on the gold core size, to know this aid in the optimization of the settings before measurements. NTA and SEM was used for this characterization and also to determine an approximative concentration of the gold nano particles. Since the NTA is not a primary technique for concentration determination, experiments were made to establish whether NTA could be trusted for this kind of measurement.

6.1.1 Size Distribution of Gold Nano Particles

In chapter 5, the manufacturing process of the gold nano particles was described. The expected size of these gold nano particles are 20-25 nm. To verify this size of the non-coated gold nano particles NTA and SEM were used. Figure 6.1 shows the NTA results for the regular gold nano particles and the PEG and PEG-biotin coated gold nano particles used for all experiments. The peaks are quite narrow which indicates a good distribution around the average size. As expected the coated gold nano particles are bigger than the non coated gold nano particles. Knowing the size difference between them gives the possibility to estimate how the coating polymer chains are orientated. The measured size difference between the coated and the non-coated are 26 nm, this indicates that the polymer chains are orientated perpendicular to the gold nano particles surface.

Comparing the size of the same gold nano particles in figure 6.1 and figure 6.2 shows that the size results in NTA are approximately 10 nm larger than in the measurement using SEM.

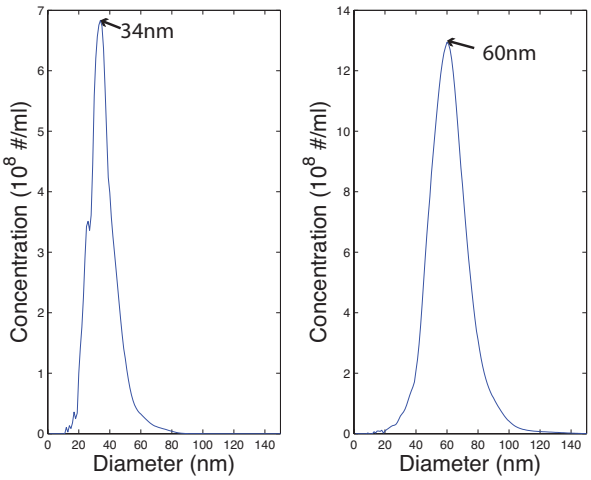

Figure 6.1: *Two NTA measurements for the same gold nano particles. One measurement for the non-coated gold nano particles (left) and one with the PEG coating (right). The gold nano particles with coating is on average* 26 nm *larger in diameter.*

This is a consistent error in this particle size range and has to be kept in mind when using the NTA system. The difference in resulting size is thought to come from that NTA measures hydrodynamic size of the particle.

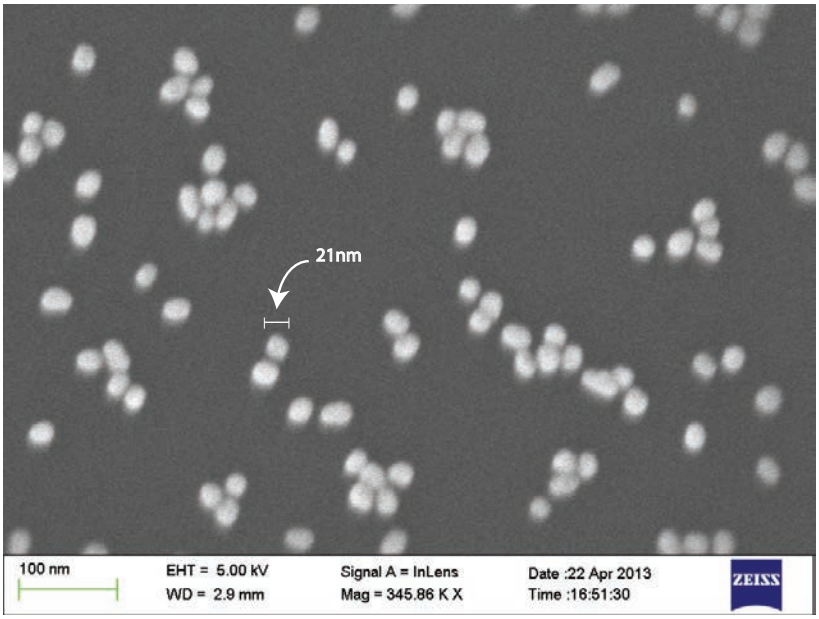

Figure 6.2: *SEM image of the gold nano particles used in QCM-D measurements as well as the waveguide system. The measured size of the gold nano particles is about 21 nm. Groupings of gold nano particles on the surface is thought to come from drying effects.*

6.1.2 Concentration Characterization

For the experiments done in this work, an approximative value for the concentration is enough. NTA is a measurement system for determining size distribution, but it can also be used to put a value on the concentration. Since measuring concentration is not what the NTA is made for a small study was done to see how accurate it can measure this. Figure 6.3 show that if the solution is in a concentration of approximately 0.2 pM the NTA can be used to determine the concentration with satisfying accuracy. There is one important aspect to keep in mind while doing these measurements, that is to choose the threshold in such a way that only particles that are in focus are traced during measurement. This could origin from that the algorithm used is based on Stokes-Einstein equation in two dimensions. In the waveguide system a concentration of approximately 6.7 pM was used.

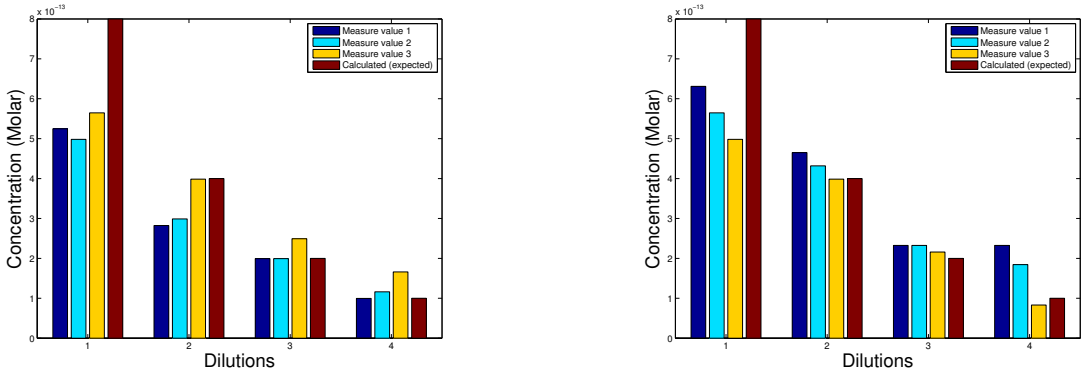

(a) Gold Nano Particles

(b) Gold Nano Particles with PEG

Figure 6.3: *Measured and calculated concentrations for two different solutions of gold nano particles with four different concentrations. The blue, cyan and yellow colors on the different dilutions are different measurement on the same concentration for better statistics. All solutions was diluted from a stock with a concentration of* 0.2 nM. *Dilutions* 1,2,3 *and* 4 *were diluted* 4/1000, 2/1000, 1/1000 *and* 1/2000 *respectively. Figure (a) shows the results with* $20 - 25$ nm *gold nano particles and figure (b) the same gold nano particles coated with polyethylene glycol making the nano particles yielding a size about* 59 nm.

6.1.3 20 nm Gold Nano Particles in the Waveguide System

After characterization of the functionalized 20 nm gold nano particles it had to be determined if the gold nano particles could be measured individually bound to the waveguide cora layer surface. To test this, the waveguide surface was functionalized with PLL and a solution of HSA and biotynilated BSA was electrostatically immobilized on the surface. Streptavidin was used as a linker between the surface and the modified gold nano particles, the system is shown in figure 6.4.

Figure 6.5 shows the individual 20 nm gold nano particles immobilized at the core layer surface of the waveguide chip. This is based on the knowledge that the gold nano particles have not aggregated at any large extent in the bulk solution and that intensity steps from the bound gold nano particles can be observed during binding. The initial image, figure 6.5 (a), contains some

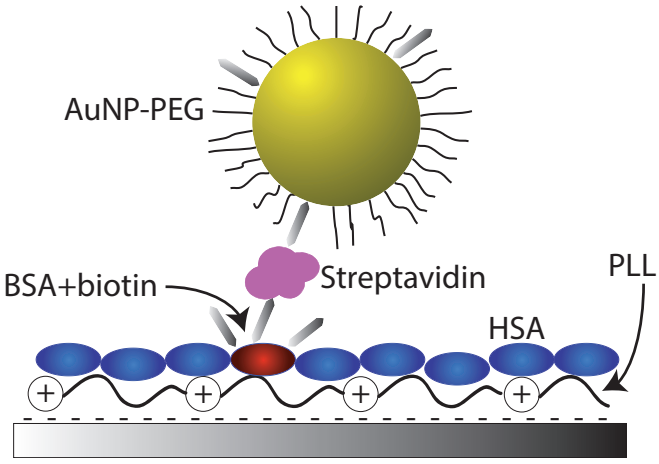

Figure 6.4: *The Poly-L-Lysine (PLL) surface functionalization for immobilization of gold nano particles to the waveguide core surface. After plasma cleaning of the surface the surface will be negative charged, the PLL is positive charged and will electrostatically bind to the surface. A solution is then added with a mixture of HSA and BSA-biotin with different concentrations of the BSA-biotin. Streptavidin is then used as a linker between the biotin on the BSA and the functionalized gold nano particles.*

spots as well. This is however not gold nano particles it is dirt either from the preparations or biological residues that did not leave the surface during the cleaning process. In figure 6.5 (b) stripes can be observed with the length period of approximately 10 μ m. These stripes are thought to origin from interference between the first and second mode in the optical waveguide. To prevent this and get a single mode waveguide work is done to tune the thickness of the core layer and obtain a single mode optical waveguide. By fine tuning the alignment of the laser fiber at the edge of the waveguide chip the stripes can be prevented, but during long measurements the laser fiber drifts and the stripes will reappear. In figure 6.6 the intensity over time can be seen for a small area where one or more gold nano particles have bounded. It can be observed that the steps in intensity are approximately multiples of each other. Even the larger steps are multiples of the single particle intensity step and could either be an aggregate or a few singular gold nano particles that bind faster then the frame rate which here is one second.

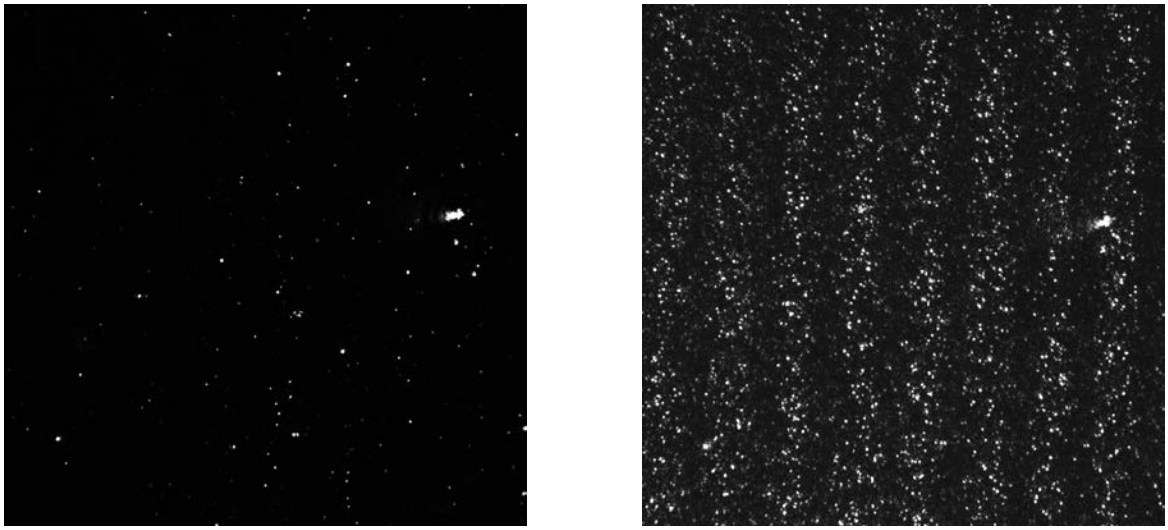

(a) Surface before injecting gold nano particles

(b) Surface after 30 min

Figure 6.5: *Images of the surface before (a) and 30 minutes after (b) the gold nano particles were added. The measurement was done with the (approx.)* 20 nm *gold nano particles that have been characterized in this section. The surface was functionlized with PLL and biotynilated BSA. Each frame is* 74 µm *by* 74 µm.

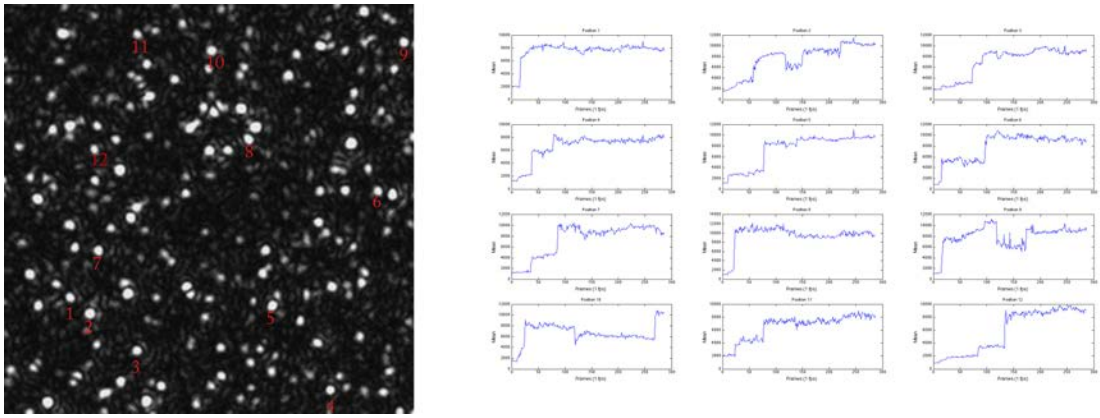

Figure 6.6: *Intensity for a few gold nano particles that bind to the surface. Each graph correspond to a small area at the numbers in the image. Looking at the intensity curves it can be observed that there are steps of around 2000 of this arbitrary unit (AU) or multiples of 2000. Since we know that the gold nano particles have not aggregated to a significant extent the conclusion is that in this experiment a* 20 nm *gold nano particle give an intensity response about 2000 AU.*

6.2 Dynamic Range Measurements

To get a feeling for the sensitivity and the dynamic range in QCM-D and to compare that to the sensitivity for the waveguide system a measurement was made to calculate the number of gold nano particles needed to get a frequency shift of one Hertz in QCM-D. The gold nano particles were immobilized using biotynilated BSA in different concentrations and the frequency shift was measured in QCM-D. The results can be seen in figure 6.7. Thereafter the same surfaces were

investigated with SEM to determine the number of gold nano particles per unit area. Figure 6.8 shows the SEM images from that measurement. Calculated from these images there would be roughly 15 000 gold nano particles per Hz in response measured with QCM-D for a area same as the measure area in the waveguide system which is 74 by 74 µm. With the most stable base line achievable in QCM-D 0.5 Hz can be distinguished. That is 7500 gold nano particles in a 74 by 74 µm frame which are not countable in the waveguide system and there for over the detection region for the system. QCM-D and the waveguide systems dynamic range is not overlapping.

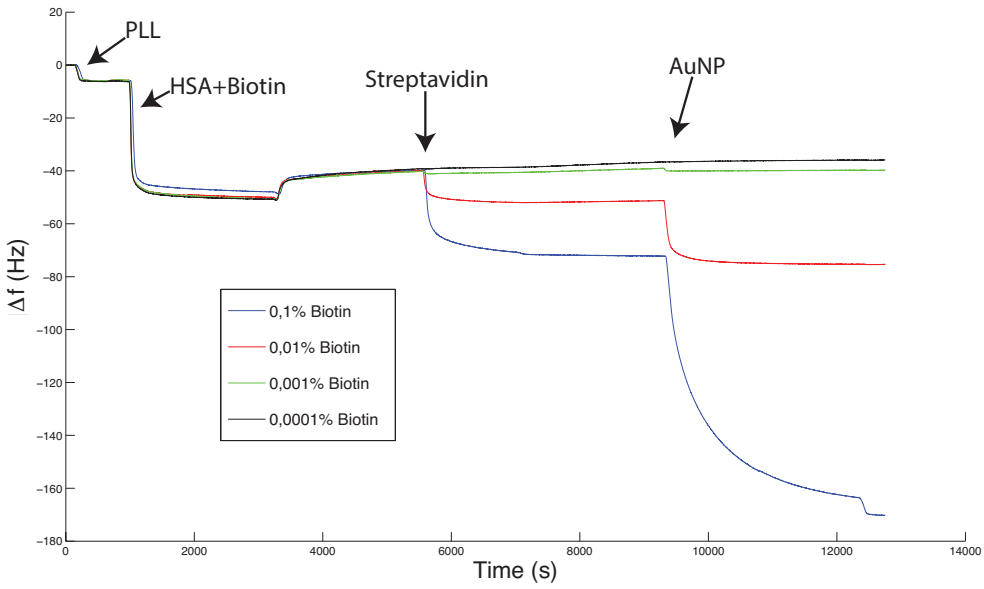

Figure 6.7: *QCM-D results from gold nano particles binding to a surface. The crystal was coated with PLL and a mixture of HSA and BSA-Biotin with different concentration was bound to the PLL. Rinsing with buffer after the solution with biotynilated BSA and HSA some of the material leaves the surface making the frequency go up. Streptavidin was then added and biotynilated gold nano particles with the same concentration for all surfaces bound to the streptavidin. SEM images of the the surfaces with the highest and lowest concentration of BSA-biotin can be seen in figure 6.8.*

6.2.1 Comparison Between Intensity and Number of Surface Bound Gold Nano Particles

During this project many experiments and measurements were carried out using the optical waveguide platform. Some for plain characterization and some to achieve and develop a sensing technique. One question was if there is a linear relationship between the intensity and gold nano particles bound to the surface. Figure 6.9 shows the number of particles binding to the surface over time and also the measured frame intensity over time. Comparing the absolute intensity changes between two different measurement carried out on two different waveguides is a bit more difficult. The scattering signal response for the gold nano particles must be roughly the same and to achieve this the settings are critical. This is sometimes preferred any way because it is much easier to determine the frame intensity than counting individual particles. Figure 6.9 shows intensity and number of particles bound to the surface corresponding to the measurement

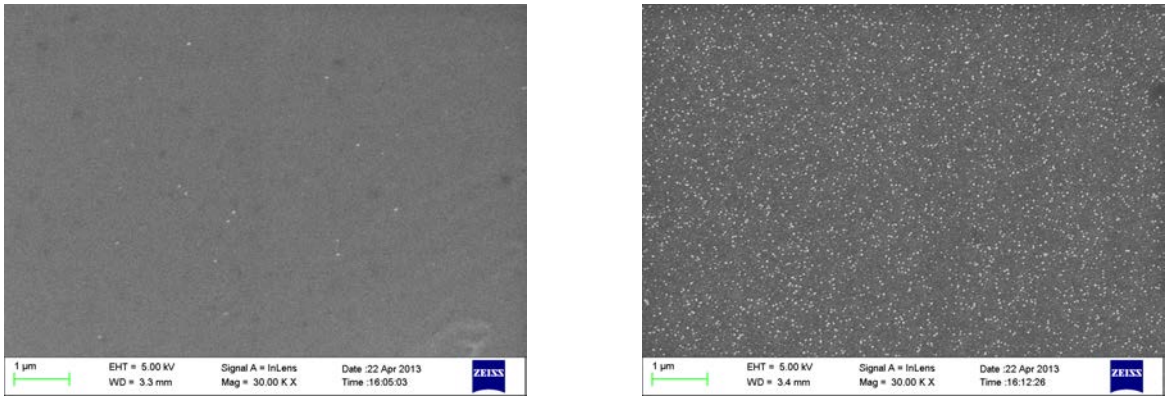

(a) QCM-D Surface with 1*ppm* Biotin

(b) QCM-D Surface with 0,1% Biotin

Figure 6.8: *Scanning electron microscope (SEM) images of the two QCM-D crystals used for binding gold nano particles, the results can be seen in figure 6.7. (a) SEM image of the crystal with* 1*ppm biotin in the HSA. (b) SEM image of the crystal with* 0,1% *biotin in the HSA.*

results in figure 6.5.

Using the combination of functionalization with PLL and blocking with HSA have been shown in this work to not be effective enough for use in the waveguide system. The biological system used for these measurements can be seen in figure 6.4. At concentrations of biotynilated BSA approximately 1000 times lower than the lowest possible concentration that could be measured with the QCM-D there were no contrast between the negative and positive control. Measurements with the waveguide system were inconsistent since the blocking was not good enough. The negative control could bind several hundreds of particles which is the same order of magnitude as the lowest concentrations examined.

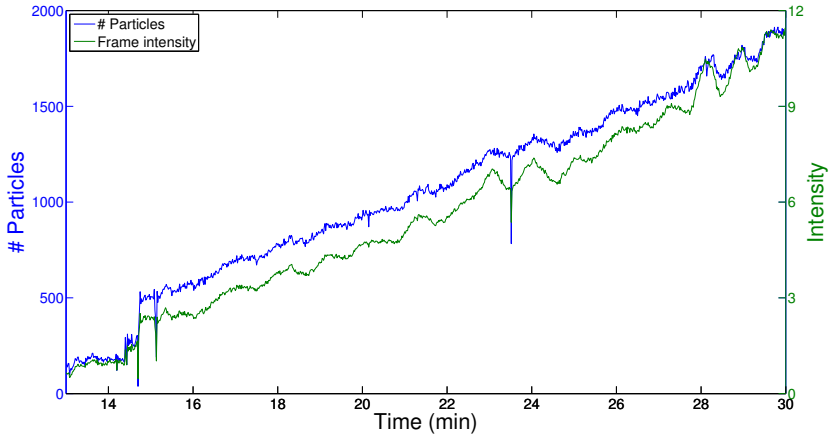

Figure 6.9: *Measurement of the number of particles in a frame and comparison with the intensity over the same frame for a image stack in a waveguide experiment. The waveguide was coated with PLL and a solution with a mixture of biotynilated BSA and HSA was added du to waveguide. Note that the intensity is an arbitrary unit and can not be compared directly to other measurements. There is a clear indication that the intensity over a frame correlates well to the number of particles bound to the surface.*

6.3 Validation of Amyloid-β 1-37 Detection using QCM-D and SPR

In order to investigate whether the biological system proposed for detection of amyloid-β could be implemented to the waveguide platform, it was first necessary to test it using reference methods. For theses reference measurements QCM-D and SPR was used. Figure 6.10 is a schematic image of this biological system which is an antibody sandwich assay. The antibody 6E10 was covalently immobilized on the surface with APDMES and glutaraldehyde whereupon the surface was blocked with HSA. Amyloid-β 1-37 is known to bind 6E10 and a secondary antibody 4G8 also bind to the peptide. The 4G8 antibody is biotynilated and streptavidin is used as a linker between the 4G8 and the functionalized gold nano particle. The measurement with QCM-D and SPR are important references to gain knowledge how the biological system behaves.

The SPR measurement was done to test if the different antibodies behaved in a similar way as described in a reference article by Muthu Ramakrishnan [19]. This was performed in order to validate the possibility to immobilize the antibody on other surfaces and keeping the functionality of the antibody. Figure 6.11 shows that this was possible and that the protocol worked well enough to proceed with. The antibody 6E10 could be immobilized and keep the functionality and binding the amyloid-β peptide. There are two different functionalization methods used in the SPR and the waveguide for immobilizing the 6E10 antibody. In the SPR measurement we used an EDC-NHS functionalization and in the waveguide APDMES and glutaraldehyde but both target the same molecular groups of the 6E10.
Figure 6.12 shows the results from the QCM-D measurement on a SOG coated crystal. The crystal with SOG and functionalized with APDMES has shown to have little to no effect on the measurement compared to a regular SiO_2 surface functionalized with APDMES. Results using

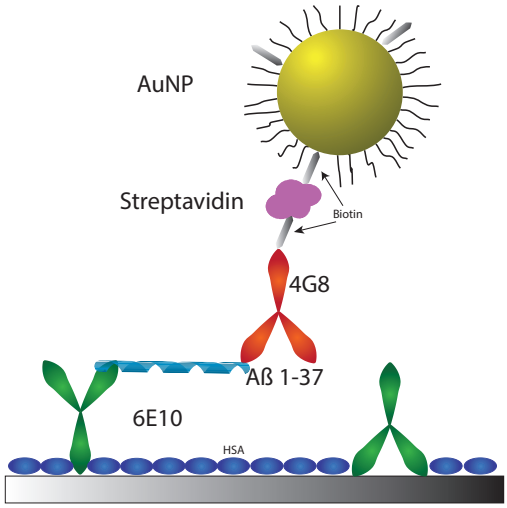

Figure 6.10: *Simple sketch of the different components of the immune assay. Antibody* 6*E*10 *is immobilized on a surface that has been silanized by APDMES and the surface is blocked with HSA. The peptide of interest, amyloid-β 1-37, binds to the* 6*E*10 *antibody but not to the HSA. Biotinylated* 4*G*8 *binds to the peptide and linked with streptavidin to a gold nano particle coated with PEG and biotin. Note that the figure is not to scale.*

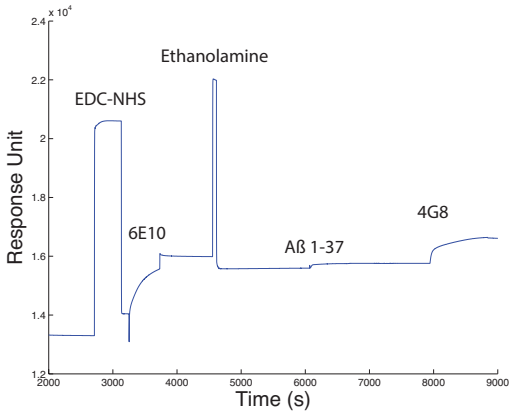

Figure 6.11: *SPR measurement with the Amyloid-β system for reference. The surface was functionalized with EDC-NHS,* 6*E*10 *is the first antibody that was immobilized to the surface. Ethanolamine was used to remove losely bound proteins on the surface. The peptide of interest, amyloid-β (*250 nM*) was then injected followed up by the secondary antibody* 4*G*8*. This measurement was done for reference to literature for behavioral properties of the two antibodies.*

QCM-D and the biological system described were easy to reproduce, the amount of antibody 6E10 and HSA was the same between repeated measurements. The measurement also seems independent of what surface is used, SiO_2 or SOG (data not shown). In the negative control no unspecific binding can be observed indicating that for this dynamic range the surface chemistry works properly.

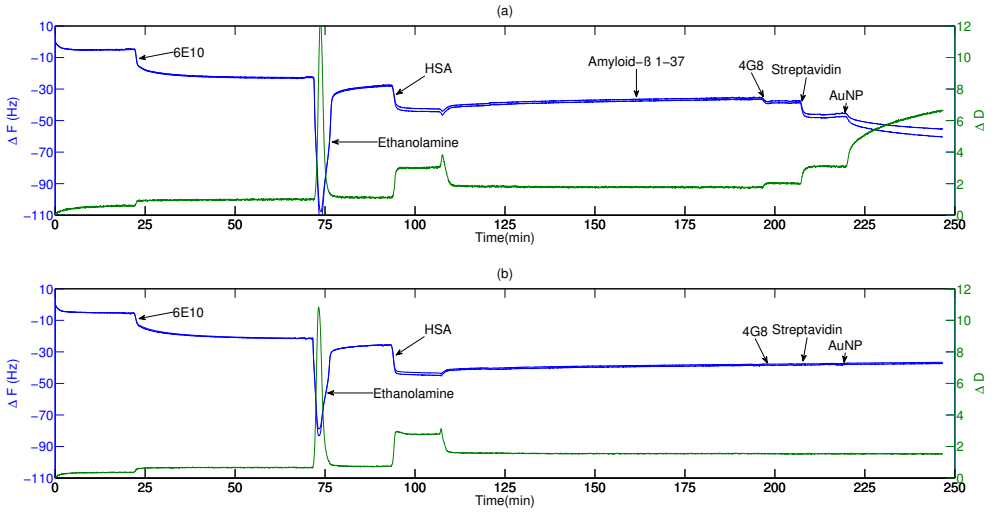

Figure 6.12: *QCM-D measurements for the amyloid-β antibody sandwich system. (a) is the positive measurement with* 250 nM *and (b) is the negative with the only difference that the amyloid-β peptide was not injected in the chamber of the negative control.The two different lines in the frequency shift is two different overtones of the vibrating crystals.*

6.4 Immuno Assay for Detection of Amyloid-β 1-37 using the Optical Waveguide System

In this section, the results from a method for detection of amyloid-β peptides are presented. Figure 6.13 show the result of the intensity measurement done on the biological system given in figure 6.10 using the optical waveguide platform. In the preparation a solution with approximately 10 nM amyloid-β peptide was added and incubated for one hour with mixing each five minutes. During the measurement no gold nano particles were observed binding in the negative control even though movement of particles could be seen coming close to the surface and then leave again, indicating a good blocking of the system surface using HSA. The result presented in figure 6.13 is shown as intensity over time because the amount of particles that bound over time was to many to be counted. As the curve in the positive control indicates the binding follows a expected behavior for particles binding to a surface.

A series of measurements with different amyloid-β peptide concentrations were made, the results are presented in table 6.1. Figure 6.14 is one of the 100 fM measurements with image that show before and 15 minutes after gold nano particles were added. This indicates that the detection region is very low, even lower than the concentrations that have been used in this experiment. Even though this is a good indicator further experiments and measurements are necessary to determine a detection limit.

Table 6.1: Number of particles counted for three different concentrations of the peptide amyloid-β 1-37 in the waveguide system. The gold nano particles were counted 10 min after they were added and the background was subtracted.

Concentration	# Particles
10 nM	>3000
1 nM	350 ± 10
10 pM	150 ± 10
100 fM	100 ± 10

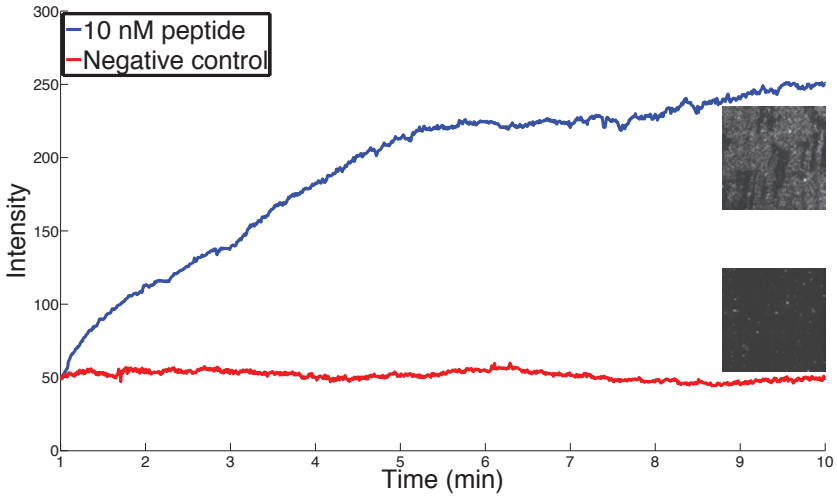

Figure 6.13: *Intensity measurement with the waveguide system of approx.* 10 nM *amyloid-β 1-37 solution compared with the negative control. The two waveguide chips were functionalized in the same manner and the biological system is the same except that the peptide has not been added in the negative control. The two insets are the surfaces at the end of the measurement.*

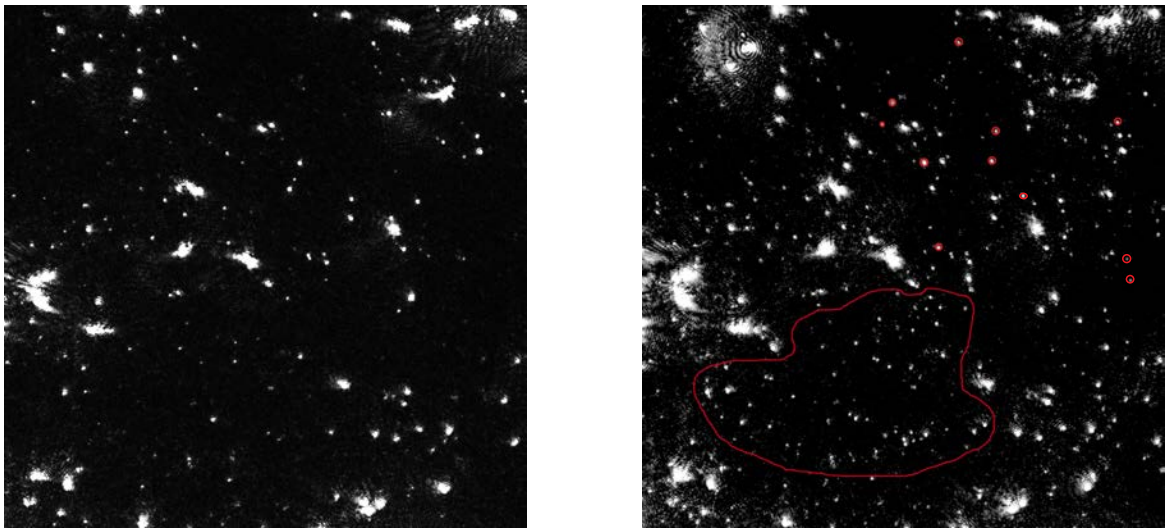

(a) Surface before injecting gold nano particles

(b) Surface after 15 min

Figure 6.14: *Measurement for detection of amyloid-β with the concentration 100 fM. The left image is before gold nano particles was added and the right image shows the surface 15 minutes after. Some gold nano particles are marked one by one and the red area is a region with good contrast and many detectible bindings.*

7

Discussion

In the work presented here there are many steps that must be individual done for each measurement, from fabrication of the waveguide platform to building up the biological system and measurements. In this chapter, results and potential errors are discussed more in depth.

7.1 Gold Nano Particle Characterization using NTA and SEM

Measuring the size distribution with the NTA is quite straightforward and reliable. Comparing the size of the gold nano particles obtained with the SEM, it is found that 10 nm have to be subtracted from the measured size obtained in the NTA to get the actual size. This has been consistent and is thought to originate from the fact that NTA measures the hydrodynamic particle size while the SEM measures the gold nano particle core. For the scattering signal observed in the waveguide system this is more relevant because the scattering of the surface functionalization on the gold nano particles will be negligible.

The use of NTA for concentration determination is not quite as straightforward. Setting the parameters in the software is much more critical, with the most critical being the threshold option. To get the most accurate result the threshold should be chosen in a way such that only nano particles in focus are measured. One possible explanation for this is that the software is, as mentioned, based on a two dimensional algorithm. Being consistent with this gives the result in figure 6.3.

7.2 QCM-D Measurements and Comparison with the Waveguide System

QCM-D is a well known and established technique and as far as equipment used it is very reliable. At the department where this project was done QCM-D is used frequently and the knowledge about the system and measurements are extensive. This is a good starting point for both preparations, experiments and discussions involving the QCM-D system. Regarding the the results this gives good confidence that no errors have been done with the aspect of the system. Meanwhile there are factors that can effect the result that can be summed up as the human factor.

Dilutions, cleaning of chambers and tubes, the miss happening of injecting air in the chamber etc.

The results obtained with the QCM-D technique shows that the functionalized gold nano particles works as probes and that the HSA works for blocking of the surface. At least at the concentrations detectible in the QCM-D system. To remember is that on a single waveguide frame the lowest amount of gold nano particles that can be detected is around 7500 for the QCM-D, which is far above the detection region with the waveguide system.

Since the results obtained from the QCM-D measurements are approximately what was expected and no errors were detected the conclusion is that the QCM-D results are valid. Unfortunately, the QCM-D results can not be compared to the waveguide system directly. The dynamic range of detection do not overlap between the waveguide and QCM-D. QCM-D has a wide dynamic range while the waveguide has not, but the waveguide has a much lower detection limit. This results in that there is no way to determine if the functionalization of the surface is good or not only that it partly has worked. A surface that gives a good result in QCM-D does not necessarily mean that it has a good surface coverage which is crucial to measure the concentrations of interest in the waveguide system.

QCM-D measurements gives a lot of positive information though. One is that the biological system, seen in figure 6.10 behaves as hoped. It gives a strong indication that the bindings are specific and that blocking with HSA to make the surface inert. We can also see that within the time of interest there are no detectible detachments from the surface. Potentially this is good for measurements in the waveguide system, since if there are no detachments only a reference image is needed before injecting gold particles and on image after a specific time.

7.3 Amyloid-β Measurements using Optical Waveguide

The waveguide system used in this project have shown great potential for measurement of molecular bindings to a functionalized surface. This could be achieved without staining the molecules with fluorophore and instead use gold nano particles as labels, scattering the evanescent field directly and monitoring with a regular upright microscope. In this section the problems and questions that we have encountered during the process are discussed.

There are differences between measuring with QCM-D and the waveguide system. In QCM-D a flow system is used for adding solutions to the chamber containing the surface this is something that we do not have in the waveguide system, all solutions were added by hand with a pipette for building up the biological system and to add gold nano particles in the waveguide system. Also with QCM-D all steps in building up the biological system can be followed in real time, this is not possible with the waveguide. The big advantage for the waveguide system over QCM-D is the low detection limit.

Fabrication of the waveguide platform is done by hand in the cleanroom laboratory at Chalmers University of Technology, Sweden. This fabrication by it self is very delicate and susceptible to errors. On several occasions it has been suspected that the surface at the sensing region is in some way not accessible for functionalization. This could have many different explanations. One is that the well has not been etched properly and that there is still CYTOP left at the surface or other residues from the fabrication. It is possible that this could happen but the explanation

has been discarded in this work because other experiments has not suffered the same problems.

A strong indication that the negative control measurement showing few or no particles bind to the surface is that the positive controls show more or less binding depending on the concentration. Zero binding has never been seen in a positive control but has been observed in negative control. The suspicion of faulty silanization came from observations in varying results of the negative control using HSA to block the surface minimizing unspecific binding to the surface. There were mainly two different result in the negative control, the expected one where very few (1-10) or no gold nano particles bound to the surface. This is of course very desired since it gives the possibility for a very low detection limit, with zero unspecific binding in theory the detection limit is infinitely low. But some times the binding was massive with several thousands of gold nano particles binding to the surface. To determine if the binding is an artifact or a good positive result for high concentration the time for the binding have to be considered. When the surface is not blocked the binding happens very fast, under 30 seconds. For high concentration with good blocking this takes a lot longer time around 10 minutes.

From this profound difference in binding behavior it can be concluded that this is a surface functionalization or blocking problem. This narrows down the possible explanations to problems with the silanization or covering the surface with HSA. Since the silane reacts with the silanols on the surface it is important that the surface is very clean. This procedure is explained in chapter 5. Due to the variating results for the negative control, it is suspected that the plasma treatment was not sufficient and/or dependent how the process was done. Previous observations from colleagues show that the efficiency of the plasma treatment are dependent on where in the chamber the sample is placed. In the work done here that has not been considered. After the plasma treatment the waveguide has also been brought through air to be rinsed with milliQ water. This could build up a monolayer of dirt from the air on the surface. Also if the waveguide is not dried properly and there are water residues on the surface this will prevent silanization. In few measurements circular dark spots have been observed, which are thought to be water residues that have prevented silanization.

If the surface observed has been properly functionalized and gold nano particles are injected without the surface being blocked massive binding to the surface is expected. The binding process here would also be very rapid. This leads to the suspicion that during the preparation of the waveguide enough HSA has reached the surface to give a proper blocking. It was thought that the relative high concentration of HSA would be enough to get a good monolayer of HSA on the surface. A fully satisfying answer to this problem has not been reached at the time of writing but there are good indications that this can be solved. This will be achieved by optimizing the process by ensuring that the plasma treatment is good, taking precautions with the rinsing with milliQ and the drying process and have a solid procedure for silanization. It has been observed that evaporating the silanes on to the surface gives a better and more even result as compared to solution based silane.

Another important source of faulty results relates to the problem of getting materials, i.e proteins and particles to the sensor interface due to diffusion limitations, which has large impact in stationary systems without controlled flow like the waveguide system. Therefore all steps except the blocking stage with HSA was mixed each five minutes with a pipet. Not mixing the HSA might have been a mistake. Also this diffusion limit could be more severe at this low

concentrations and volumes. To exemplify this think about the experiment with the 100 fM amyloid-β solution. In this experiment approximately 100 gold nano particles bound to the 74 µm by 74 µm frame. The well is 2 mm by 2 mm, which gives approximately 730 measurement frames which results in total 73 000 molecule bound to the well bottom surface. In the solution on the well there are about 1 800 000 peptides in total this gives that the concentration has gone down about 4%. This is the theoretical case. The peptide can also stick to other surfaces during this process for example in the mixing of the solution the peptide can stick to inner walls of the container tube used for mixing the solution, or the inside of the pipet tips. This is especially critical at this low concentrations.

All handling of the sample is a potential risk. This includes the rinsing and mixing of the sample in each step. It is a bit harder than one might think, by mistake it is very easy to scratch the surface with the pipet tip. What effect this kind of contact has is not totally clear but should be avoided.

Measurement with the waveguide system is not as straight forward as compared to the QCM-D. There are many different parameters that have to be considered before starting a measurement. Laser power, laser fiber alignment, exposure time, gain, find a good place etc. must be optimized. One major problem is the stripes observed in figure 6.5, at the time this is written there are no satisfying explanation for this. They can be avoided by finding a very small interval in the z-direction of the laser fiber. This is not always easy and over time they can reappear due to drift in the micro screws used to align the fiber.

A good illumination and exposure settings are important to be able to process the gathered images. To get the optimal signal to noise ratio the bound gold nano particles should not saturate but be just below saturation to use the dynamic range the camera have to offer.

7.4 Image and Data Processing

For image processing the free software *ImageJ* has been used. It is a great tool for handling image stacks and processing images but can sometimes be hard to handle for good results. Using the particle count plugin in ImageJ a threshold must be chosen for at what intensity peaks will be counted as particles. There are a couple of things that can go wrong here and must be kept in mind. One thing that must be considered is the illumination varying in time. If it is, particles that have been counted in one frame could not be counted in the next even if the particle is still attached to the surface due to that the drop in illumination makes the particle go under the set threshold. The intensity can be corrected by choosing a particle on the surface that one would guess should not change its intensity over time and use that to correct for intensity drift. Unfortunately there are local changes in intensity as could be seen in figure 6.5. These stripes can move over time making it very hard to make corrections in a good way.

8

Conclusion

In this work 20 nm surface functionalized gold nano particles were successfully visualized bound to a streptavidin modified surface using a regular upright microscope, 532 nm laser and a planar symmetric optical waveguide. The gold nano particles were bound to the functionalized core layer of the waveguide where they could be visualized due to their ability to scatter the evanescent field on the surface. Measurements were done in liquid and in real time making it possible to determine if a gold nano particle bound reversible or irreversible.

Comparing the dynamic range of the waveguide with the dynamic range of QCM-D it is shown that the waveguides highest range of bound gold nano particles that could be measured is around one order of magnitude lower then the lowest possible detection of gold nano particles with QCM-D. Since the waveguide in theory has an infinitely low detection limit a lot of work have been done regarding the surface chemistry and on improving the background signal. With proper silanization and covalently bound HSA as a blocking agent a good inert surface was achieved. This was not the case when the surface was functionalized with PLL and HSA was electrostatically bound down to the surface. To get material, different molecules and gold nano particles, down to the surface mixing the solution is of great importance. We also saw that even at relative high concentrations it can be difficult to get material down to the surface due to diffusion limitations.

A biosensing technique for detection of amyloid-β was developed based on an antibody sandwich and using biotynilated gold nano particles as labels. Using this biological system on the waveguide, concentration down to 100 fM of amyloid-β 1-37 could be detected.

9

Future Perspectives

Even though the results presented here are very promising there are a lot of more work that could be done. Both to validate the results further, but also there is a lot of potential in the system presented in this work.

9.1 Solving Blocking and Functionalization Problems

As mentioned in the chapter 7 there has been some problem with blocking the surface and making the measurements consistent. This problem is thought to arise due to a systematic error and should be able to be solved. To do this every step should be validated more in detail then time have allowed in this work. Maybe the most critical is the examine the plasma cleaning and the protocol of cleaning the waveguide platform. Evaporation of silan on the surface to get a more homogenous silan monolayer should also be investigated further.

9.2 Multiple Wavelength Measurements for Ratio Determination of Different Amyloid-β Peptides

In the optical waveguide system multiple lasers can be used for illumination. This gives the opportunity to use different label nano particles for different molecules binding to the surface. Using silver nano particles and gold nano particles with green and blue laser will make it easy to distinguish two different molecules binding to the surface.

This could be used for example to measure the ration between amyloid-β42/amyloid-β40 peptides mentioned in the introduction. Hopefully this can be done just by analyze the RGB values of a single frame.

9.3 Smartphone Applications

By using a regular smartphone, the optical waveguide platform, laser and cheap ”toy” optics images on surfaces covered with 65 nm can be seen in figure 9.1 and 9.2. Hopefully this can be used to create a cheap method and device to be able to detect different molecules in solutions.

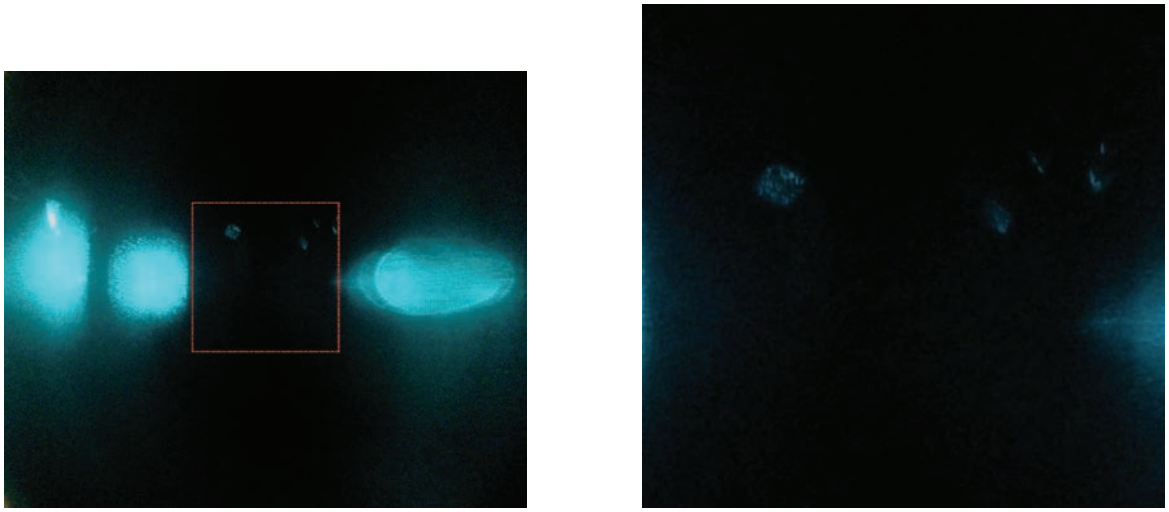

(a) Full image of the negative control

(b) Well crop of negative control

Figure 9.1: *The image of the negative control sample. (a) is the full image from the iPhone and (b) is the well cropped out digitally, the area is indicated by the red dotted line. Here there is a very low intensity indicating that no gold nano particles or very few have bound to the surface.*

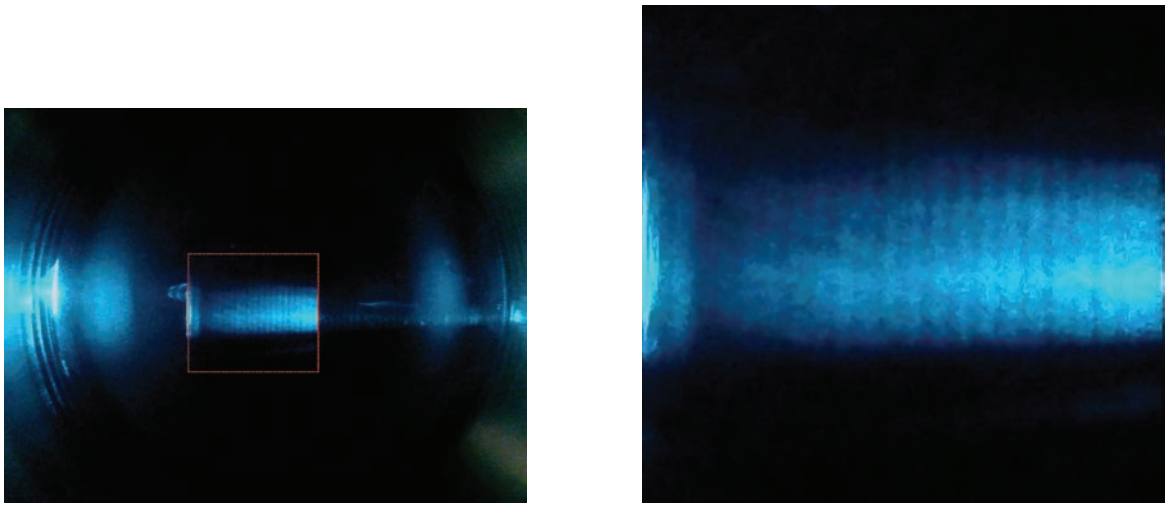

(a) Full image of the positive control

(b) Well crop of positive control

Figure 9.2: *Image of the positive control with 65 nm gold nano particles bound to the surface. (a) is the full image and (b) is the well cropped out digitally, the area is indicated by the red dotted line.*

Bibliography

[1] McManus, T. (2009) The future of mind-controlled prostheses. *O & P Business News : Linking the Orthotic and Prosthetic Profession* **18**, 20–22,24. Copyright - Copyright SLACK INCORPORATED Oct 15, 2009; Last updated - 2010-06-06.

[2] Zetterberg, H. (2007) Identification of a beta]-amyloid-binding plasma protein, lrp1: implications for biomarker research and therapy in alzheimer's disease. *Biomarkers in Medicine* **1**, 347–8.

[3] Blennow, K, de Leon, Mony, J, & Zetterberg, H. (2006) Alzheimer's disease. *The Lancet* **368**, 387–403.

[4] Blennow, K, Zetterberg, H, & Fagan, A. M. (2012) Fluid biomarkers in Alzheimer disease. *Cold Spring Harbor perspectives in medicine* **2**, a006221.

[5] Sagare, A, Rashid, D, Bell, R. D, Johnson, B, Hamm, K, Pendu, R, Marky, A, Lenting, P. J, Wu, Z, Zarcone, T, Goate, A, Mayo, K, Perlmutter, D, Coma, M, Zhong, Z, & Zlokovic, B. V. (2007) Clearance of amyloid-beta] by circulating lipoprotein receptors. *Nature medicine* **13**, 1029–31.

[6] Axelrod, D. (1989) in *Fluorescence Microscopy of Living Cells in Culture Part B. Quantitative Fluorescence Microscopy–Imaging and Spectroscopy*, Method. Cell Biol., eds. Taylor, D. L & Wang, Y.-L. (Academic Press) Vol. 30, pp. 245–270.

[7] Agnarsson, B, Ingthorsson, S, Gudjonsson, T, & Leosson, K. (2009) Evanescent-wave fluorescence microscopy using symmetric planar waveguides. *Optics express* **17**, 5075–82.

[8] Phillips, R, Kondev, J, & Theriot, J. (2009) *Physical Biology of the Cell.* (Garland Science).

[9] Jones, R. A. L. (2011) *Soft Condensed Matter.* (Oxford University Press).

[10] Bongrand, P. (1999) Ligand-receptor interactions. *Rep. Prog. Phys* **921**.

[11] Glenner, G. G & Wong, C. W. (1984) Alzheimer's disease: initial report of the purification and characterization of a novel cerebrovascular amyloid protein. 1984. *Biochemical and biophysical research communications* **425**, 534–9.

[12] Janshoff, a, Galla, H, & Steinem, C. (2000) Piezoelectric Mass-Sensing Devices as Biosensors-An Alternative to Optical Biosensors? *Angewandte Chemie (International ed. in English)* **39**, 4004–4032.

[13] Sauerbrey, G. (1959) Verwendung von schwingquarzen zur wagung dunner schichten und zur mikrowagung. *Zeitschrift Fur Physik* **155**, 206–222.

[14] Cooper, M. a. (2004) Advances in membrane receptor screening and analysis. *Journal of molecular recognition : JMR* **17**, 286–315.

[15] Rodahl, M, Höök, F, Krozer, A, Brzezinski, P, & Kasemo, B. (1995) Quartz crystal microbalance setup for frequency and Q-factor measurements in gaseous and liquid environments. *Review of Scientific Instruments* **66**, 3924.

[16] Brändén, M, Tabaei, S. R, Fischer, G, Neutze, R, & Höök, F. (2010) Refractive-index-based screening of membrane-protein-mediated transfer across biological membranes. *Biophysical journal* **99**, 124–33.

[17] Saveyn, H, De Baets, B, Thas, O, Hole, P, Smith, J, & Van der Meeren, P. (2010) Accurate particle size distribution determination by nanoparticle tracking analysis based on 2-D Brownian dynamics simulation. *Journal of colloid and interface science* **352**, 593–600.

[18] Dragovic, R. a, Gardiner, C, Brooks, A. S, Tannetta, D. S, Ferguson, D. J. P, Hole, P, Carr, B, Redman, C. W. G, Harris, A. L, Dobson, P. J, Harrison, P, & Sargent, I. L. (2011) Sizing and phenotyping of cellular vesicles using Nanoparticle Tracking Analysis. *Nanomedicine : nanotechnology, biology, and medicine* **7**, 780–8.

[19] Ramakrishnan, M, Kandimalla, K. K, Wengenack, T. M, Howell, K. G, & Poduslo, J. F. (2009) Surface plasmon resonance binding kinetics of Alzheimer's disease amyloid beta peptide-capturing and plaque-binding monoclonal antibodies. *Biochemistry* **48**, 10405–15.